Applied Physics A (2022) 128:591
https://doi.org/10.1007/s00339-022-05720-9

Applied Physics A
Materials Science & Processing

Rheological investigation of strain rate and magnetic field on the magnetorheology of zinc ferrite ferrofluid

A. Abideen Ibiyemi[1] · **Gbadebo Taofeek Yusuf**[2]

Received: 24 March 2022 / Accepted: 22 May 2022 / Published online: 18 June 2022

Abstract

The major problems disturbing the rheology of magnetic fluid are deformation of magnetic aggregate and destruction of field-induced structure, and this has caused major drawbacks to the rheological systems. The magnitude of the deformation is dependent on the percentage of the strain rate. To curtail the drawback and improve the rheology of the magnetic nanofluid, low strain rate application is required for fluid material testing. Henceforth, we examine the effect of strain rate and magnetic field on the rheological properties of zinc ferrite ferrofluid (FF) using oscillatory sweep test. The rheology of the fluid is examined in the absence and presence of magnetic field at strain amplitude 1%, 10%, 33%, and 100%. The magnitude of the deformation varied as the strain percentage is altered. Low deformation is formed at strain 1% and 10%, this results to the formation of improved and better rheological systemic function, and the rheological function is partially weakened at strain 33%, whereas structural deformation is higher at strain 100%. At strain 100%, the rheological system is largely weakened, but at strain 1%, the rheological system is enhanced. At low strain, high complex magnetoviscosity, low shear stress, low rotating magnetic field, and improved viscoelastic system are formed, but, at high strain application, low complex magnetoviscosity, high shear stress, speedy rotating magnetic field and poor viscoelastic system are formed. A steady-state flow is formed when low relaxation modulus is applied. At high strain, high rotation is formed, and this breaks the rotating magnetic field and destroys the magnetic structure, but at low strain, the rotation of the rotating magnetic field is low, and this protects the aggregates from destruction. The synthesized particles were ultra-sonicated and coated with oleic acid to curtail agglomeration of the particle. The storage modulus (G') is largely greater than loss modulus, and this established the formation of dominant elastic structure. From TEM analysis, a spherically shaped nanoparticle is formed. The XRD analysis indicates the formation of cubic structure and Fe-phase in trivalent state. The hopping lengths in the tetrahedral site A and octahedral site B are 3.61 nm and 2.94 nm, while the lattice parameters a and c are 8.3298 Å and 13.7501 Å.

Keywords Strain rate · Complex viscosity · Torque · Magnetization · Coercivity · Shear stress · Modulus

1 Introduction

This research accurately examines the effect of strain rate on the rheology of zinc ferrite nanofluid. Reports show that shear strain is useful in changing the dimensions of fluid particle structure upon the application of stress, and the dimension of particle structure is changed or deformed base on the percentage of the strain. In fluid mechanics, when shear stress acts upon the fluid flowing, the percentage of the shear strain is actually significant, because fluid is progressively deforming due to increasing shear strain. The rate of deformation is dependent on the percentage of the strain. If a material is acted upon by low strain rate, the dimension of the fluid structure does not significantly change, and this implies the formation of minimal deformation [1, 2]. However, if material is acted upon by high strain rate, the dimension of the fluid structure significantly changes, and this illustrates the formation of maximal deformation [1–3]. According to Yang et al., Ibiyemi et al., and Maurya et al., strain deformation is higher at high strain rate region, whereas strain deformation is low at low strain rate region; this occurred due to difference in dimensions of the fluid structures. One of the purpose of this study is to examine the

✉ A. Abideen Ibiyemi
abideen.ibiyemi@fuoye.edu.ng

[1] Department of Physics, Federal University, Oye-Ekiti, Nigeria

[2] Department of Science Laboratory Technology, Osun State Polytechnic, Iree, Nigeria

strain rate sensitivity on the viscosity and elastic nature of the fluid. In 2022, Maurya and Sarkar reported that the shear stress is increased with increasing strain; this closely agrees with our present findings. This also agrees with experimental findings reported by Yang et al. Ibiyemi et al. reported that ferrofluid is strain sensitive, and the research team showed that at low strain, the fluid is dominated with elastic structure and exhibits solid-like nature. Enhanced elastic structure is formed due to minimal deformation of fluid structure. However, at high strain application, the elastic structure is destroyed, and the structure of the fluid is largely deformed due to high strain application.

In the presence of magnetic field, the magnetic-induced aggregate destroys at high strain; this occurred, because the magnetostatic force is not susceptible of resisting the effect of high strain, and the magnetic structure is henceforth destroyed. However, at low strain rate, the magnetic aggregate does not destroy; this occurred, because the low strain application is not susceptible of destroying the magnetic aggregates. Ibiyemi et al. reported the formation of crossover between the storage modulus and loss modulus, and the crossover point illustrates the point at which the elastic microstructure of the fluid particles is destroy at high strain region. The formation of crossover point reveals the formation of phase transition from solid-like state to liquid-like state. Chattopadhyay et al. reported the formation of elastic dominant system at low strain region; at this region, the storage modulus is higher than the loss modulus. The system becomes viscous dominated at high strain rage region [4]. Similar experimental observation was reported by Prasad and Gangadharan in 2014 [5]. Yongbo et al. reported experimental finding which precisely conform to our result, because storage modulus is extremely dominant over loss modulus; this suggests the formation of elastic dominant structure and solid-like magnetorheological fluid [6]. Mitsumata and Okazaki [7] reported the dependent of storage modulus on strain rate, the storage modulus is diminished as the strain rate is increased, and this result accurately conforms to result reported from current findings. Zukas and Tailor examined the effect of strain on the plastic and elastic structure of iron; it was reported that at low strain, elastic structure is formed, whereas plastic structure is formed at high strain rate. This experimental result cordially agrees with our findings [8].

Details from present experimental findings revealed the formation of enhanced rheological characteristics at low strain rate; this is formed due to formation of higher magnetoviscosity, low shear stress, low rotating magnetic field, and improved viscoelastic system. However, at high strain rate, the rheological system is weakened; this occurred, because the system exhibits lower magnetoviscosity, high shear stress, speedy rotating magnetic field, and poor viscoelastic system. At low strain rate, the system exhibits low structural deformation due to the effect of low shear stress, the low shear force cannot withstand the magnetostatic forces binding the particles together, and this protects the particle aggregates from destruction. While at higher strain rate, the magnetic structure is completely deformed; this occurred due to high strain application which completely destroys the magnetic aggregates. The destruction of the magnetic aggregate leads to formation of extremely low magnetoviscosity.

Magnetorheological fluids (MRF) are a typical smart magnetic material that exhibit the characteristics that specially show response to phase transition from liquid state (viscous) to a semi-solid state (elastic), and MRF reveal magneto rheological effect under the application of magnetic fields. MRF exhibit useful properties and has typical features that links with mechanical systems such as vibration and torque transmission. The typical mechanical systems include hydraulic system, brakes, seismic vibration dampers, shock absorbers, clutches, control valves, and artificial joints [9]. Some other applications of magnetic fluid include isothermal magnetic advections [10], precision polishing [11–13], biomedical applications [14], sound propagation [15], and chemical sensing applications [16, 17], and all these applications involve the use of magnetic field. Some other reports showed that ferrite nanoparticles are useful as gas sensors [18], magnetic substance [19, 20], ferrofluids [21], microwave [22], and transformer cores [23]. Ferrite (Fe_2O_3) can be used in creating a nanocomposite purposely for the formation of hydrogen storage and photocatalytic activities. The photocatalytic activity involves the removal of water contaminant, and this application was formed by mixing ferrite (Fe_2O_3) with certain compound such as $EuVO_4$ and g-C_3N_4 [24]. Monsef et al., reported in 2021, that ultrasonic treatment of Fe_2O_3 nanostructure can accurately restructure the structural and magnetic behavior of ternary composite at nano-range. A nanocomposite $EuVO_4$/g-C_3N_4 mixed with Fe_2O_3 exhibits a large hydrogen storage capacity and better photocatalytic activity. The coexistence of ferrite with $EuVO_4$/g-C_3N_4 nanocomposite can be used for water treatment via photocatalytic system [24]. The formation of enhanced electro-catalytic activity was also reported by Monsef et al., and the research team also reported the use of magnetic Fe_2O_3/$EuVO_4$/g-C_3N_4 nanocomposite for electrochemical activities. Another report from Zinatloo-Ajabshir shows that the composite of cobalt ferrite is useful as photocatalyst for the degradation of organic contaminant. Cobalt ferrite that coexists with tin oxide (TiO_2) and $Dy_2Ce_2O_7$ can also be used for removal of water contaminant [25]. Various methods have henceforth been used by various research teams for the synthesis of ferrite magnetic samples. Kombaiah et al. used microwave-assisted combustion to synthesize $ZnFe_2O_4$, and other methods reported include thermal decomposition, sol–gel, co-precipitation, ball milling, oxidation, and hydrothermal [26–33].

When magnetic particles are dispersed in a liquid medium, a stable, non-concentrated nanomagnetic fluids known as ferrofluid is formed. In consideration of the particle size, concentration of the fluid particles, and the nature of the carrier medium, the rheological effect of the magnetic fluid such as Newtonian or non-Newtonian behavior is formed regardless of whether external magnetic field is applied. The magnetic size of the nanomagnetic particles is dependent on the structure of the external magnetic field [34]. Magnetic structure such as chain-like aggregate is formed when magnetic field is applied, and study shows that the nature of the chain-like aggregates is dependent on the strength of the applied magnetic field. Result from this work shows that the strength of the magnetic structure determines the rheological performance of the concerned magnetic fluid. Illustrations from existing literature show that rheology of the magnetic fluid is based on relevant factors such as the magnetic field, strain rate, shear rate, surfactant, and particle concentration. Under certain condition, the rheological properties of the magnetic fluid are dependent on the shape of the disperse phase [35]. The magnetorheological effect of the ferrofluid is mostly attributed to the formation of field-induced magnetization of the suspended nanomagnetic particles. The particle suspensions exhibit a relatively low viscous effect in the absence of magnetic field due to non-formation of field-induced magnetization and the particles are not magnetically interacted. In the presence of magnetic field, the particles are magnetized, and interact with one another along the direction of the magnetic field and form anisometric particle aggregates that traverse the system.

Recent studies show that rheological properties can be modified by optimizing the synthesis parameters. The properties are modified to create better nanofluid environment. Several measures have henceforth been taken to ensure the formation of better magnetic fluid, one of which is to create a stable fluid environment which has been very difficult to form. However, the formation of the nanofluid is being faced with drawback due to formation of particle coagulation, and this typically affects the fluid stability. Coagulation of particle affects the settling rate of the particles and restricts the fluid performance [36]. Several measures have hence been taken to lower the settling rate of the fluid particles, one of the measures include coating the fluid medium with liquid surfactant such as oleic acid, and this creates enabling environment that reduces the settling rate of particles of the nanofluid to lowest minimum in such a way that the particles are well dispersed in the fluid medium [37]. Other measure includes the application of magnetic field; upon the application of magnetic field, magnetic particles are polarized; the magnetic particles are binded to their respective aggregates and form chain structures from which number of cavities are created. The cavities are filled by particles and form a nanobridge of colloidal system [38]. The rheological properties of the nanofluid are improved due to formation of stable fluid environment, and the stable nature of the fluid makes it to be useful in various device applications, such as lubricants, dampers, bearings, and clutches [39].

This research work focuses on the synthesis of zinc ferrite magnetic nanofluid and examines its rheological effect. The magnetoviscosity and the viscoelastic properties of the synthesized fluid are examined both in the absence and presence of magnetic field. The effect of strain rates on the magnetorheological properties is also examined. The main significance of this findings is to establish a suitable condition required for the formation of enhanced rheological effect. From our result, we see that enhanced rheological system is formed only with minimum structural deformation, and this deformation is dependent on the percentage of the strain rate. Via minimum deformation, enhanced magnetoviscosity, small rotating magnetic field, and low shear stress are utmostly formed. Literature show that most findings are only based on investigation of fluid rheology under the application of single strain rate, most findings are based on strain rate 100%, and this implies that the structural deformation has not been actually controlled based on the strain rate effect. In our study, different strain rates are employed; this allows us to control the deformation caused by strain rate effect. The application of varying strain rate can be actually used to monitor and control the deformation of structure. The structural deformation is controlled through the application of varying strain rate. Although, a lot of studies have been carried out purposely to monitor deformation but based on other parameters, such as magnetic field strength, shear rate, material structure, etc. Prior the analysis of rheological properties, the particle microstructure and surface morphology is determined using X-ray diffraction technique (XRD) that operates with CuKα radiation in the 2θ range of 10°–80° with step size 0.02° in a continuous scan mode with scan speed 3000: Scanning Electron Microscopy (SEM), Transmission Electron Microscopy (TEM), and High Resolution Transmission Electron Microscopy (HRTEM). The atomic composition and optical effect of the fluid particles are examined using Fourier Transform Infrared (FTIR) and Photoluminescence Spectroscopy (PL). The magnetic elements such as saturation magnetization, remanence magnetization, and coercivity are examined using Vibrating Sample Magnetometer (VSM).

It has been accurately established that micro-structured materials exhibit remarkable physico-mechanical properties, such as elasticity, stiffness, hardness, etc. The implementation of a suitable size-dependent elasticity theories to properly examine the physico-mechanical response of zinc ferrite microstructure is proposed for future research findings. Since present work is purely experimental, we therefore propose to implement some mathematical models to validate already

conceived experimental results. Our proposition involves the use of higher order elasticity theory which presents significant evidence of accurately established size-dependent elasticity models such as modified nonlocal strain gradient model, strain gradient model, and nonlocal strain-driven gradient model. These originated higher order elasticity models can be accurately use to examine the structural property of magnetic nanofluid and characterize the structural compositions of cutting edge nanostructures as reported by Faghidian in 2021 [40]. In 2021, Faghidian reported that two frameworks which include nonlocal elasticity model and gradient elasticity theory have been extensively used by various researchers to fine-tune the physico-mechanical responses of materials at nano-range. Faghidian also reported that physico-mechanical properties such as stiffening and softening of structures can be accomplished using augmented elasticity theory [41]. Faghidian also reported that nonlocal modified gradient elasticity theory can be used to provide a practical proposition to examine the nano-outlook of the field quantities. In 2021, Faghidian used flexure mechanics of nonlocal modified gradient to accomplish the structural responses of physico-mechanical characteristics such as stiffening and softening at nano-range [42]. Nonlocal modified gradient theory can be used in nano-scopic study of dynamic and static characteristics of nano-scale elastic material [42]. Since zinc ferrite ferrofluid is dominated with elastic structure, nonlocal modified gradient theory is accurately fit for investigating the elastic nature of the structure. Other report from Faghidian illustrates that higher order mixture nonlocal gradient theory of elasticity was formulated by means of consistently unifying nonlocal elasticity, and this unify model is suitable for examining the micro-elastic structure of fluid [43]. Similar scientific fact was reported by Faghidian in 2022, and he reported that the nano-scopic response of advanced nano-materials can be characterized using generalized gradient elasticity theory [44].

2 Methodology

Figure 1 shows the schematic diagram of the experimental procedure of zinc ferrite ferrofluid. The required solution used to synthesis zinc ferrite magnetic nanoparticles is formed by mixing anhydrous iron (III) chloride ($FeCl_3$) and zinc (II) chloride hexahydrate ($ZnCl_2.6H_2O$). Prior the synthesis of the zinc ferrite particles, the beakers were cleaned using deionized water and later rinsed using acetone. The beakers were cleaned to get rid of impurities that could be present in the beakers. All chemicals were procured from Merck Chemicals. We obtain deionized water (DI) using SHRO-plus DI (18 MΩ) system. Zinc ferrite nanomagnetic particles were synthesized using chemical co-precipitation technique. Aqueous salt solutions of Zn^{2+} and Fe^{3+} ions in the ratio of 1:2 were employed. The needed amount of aqueous solutions was weighed using digital weighing balance, dissolved it in deionized water, and heated for 30 min at

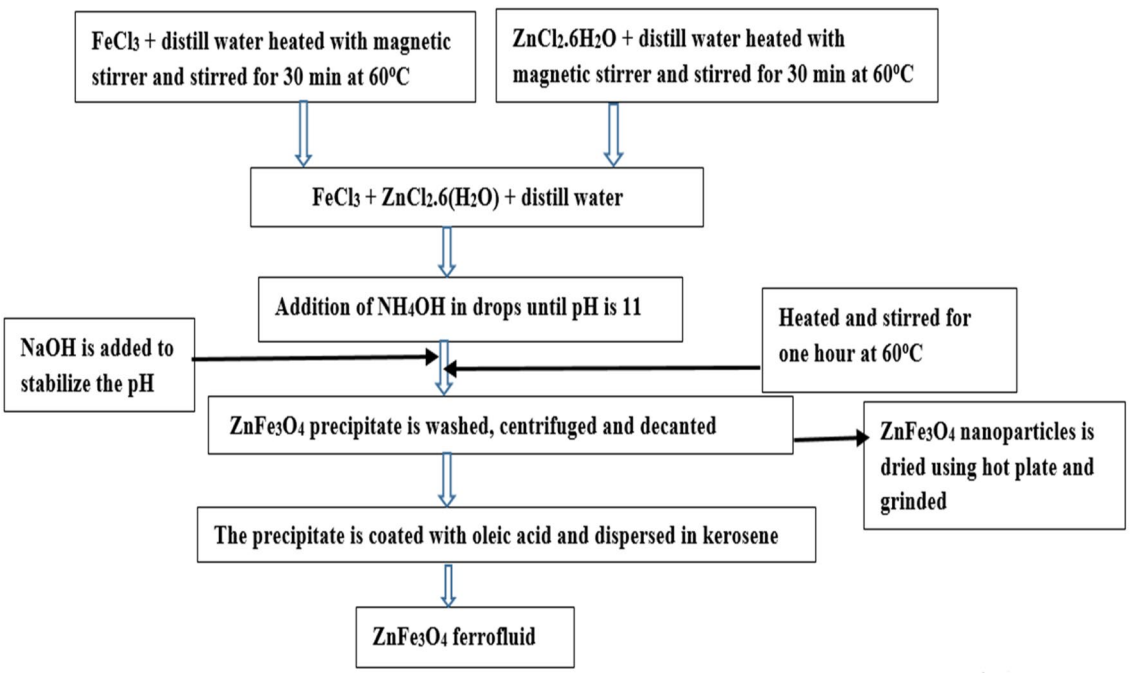

Fig. 1 Schematic diagram of experimental procedure of zinc ferrite ferrofluid

60 °C using magnetic stirrer in a separate beaker. The solutions were stirred to form homogeneous solution. The solutions containing Zn^{2+} ions and Fe^{3+} ions were later mixed together and heated for 1 h. Ammonia solution was added in drops to obtain precipitate until a pH 11 is formed. One mole of sodium hydroxide (NaOH) is added to the mixture of Zn^{2+} and Fe^{3+} to stabilize the pH of the liquid solution. After the formation of the zinc ferrite particle, the precipitates were carefully washed severally and treated via decantation process. The precipitate was coated with oleic acid and stirred for 15 min. The coated particles were filtered and washed with deionized water and acetone to get rid of all kind of impurities. The particles were dispersed in kerosene and form a wet slurry. The slurry was centrifuged at 12,000 rpm to obtain smaller size particles; this is to ensure the separation of larger particle sizes; therefore, $ZnFe_2O_4$-based ferrofluid was obtained. The X-ray diffraction patterns were obtained using Rigaku Ultima multiple X-ray diffractometer. The Scanning Electron Microscope was used to obtain the particle morphology and microstructure. The absorption bands were determined using Fourier Transform Infrared (FTIR) spectrometer, the atomic composition was carried out using Energy-Dispersive X-ray Spectroscopy, and rheological properties were investigated using an MCR-301 rheometer (M/s Anton Paar).

3 Results and discussion

3.1 Energy-dispersive X-ray and X-ray diffraction analysis

The elemental composition of zinc ferrite powder was examined by energy-dispersive X-ray spectroscopy. Similar technique was used by Hassanpour et al. [45] and Ghiyasiyan-Arania et al. [46], to investigate the element and the composition of Co_3O_4/ZnO and $FeVO_4/V_2O_5$ nanocomposite. The result obtained from EDS is illustrated in Fig. 2a. The spectral shows the presence of zinc, iron and oxygen in different proportion. The atomic weight of Zn^{2+} ion composition from EDS analysis does not agree with the composition used during synthesis. This might be due to partial substitution of Zn^{2+} ions into Fe^{2+} interstitial lattice which possibly result to the formation of concentrated Fe^{3+} particle as revealed by the histogram representation of the atomic weight in Fig. 2b. Also, the Zn^{2+} particles might possibly occupy oxygen vacancies in the lattice, and the vacancies act as trap center for charge carriers which is helpful in reducing electron hole recombination. The EDS revealed the absence of foreign element (impurity); this shows that the synthesized nanoparticles is 100% pure.

The structure of zinc ferrite powder was examined using X-ray diffraction technique. Similar technique was used by Zinatloo-Ajabshir et al. [47], Panahi-Kalamuei et al. [48], Davar et al. [49], and Monsef et al. [50], to investigate the structural properties of Nd_2O_3-SiO_2 nanocomposites, SnO_2 nanoparticles, CeO_2 nanoparticles, and $V_{3.6}Mo_{2.4}O_{16}$–chitosan (MV-CHT) nanocomposite. Figure 2c illustrates the XRD patterns of zinc ferrite sample, and the X-ray shows the formation of single-phase cubic spinel structure. The diffraction peaks correspond with the cubic structure of $ZnFe_2O_4$ (ASTM card no.: 22-1086) and the peaks were obtained at various diffraction angles: 29.258°, 35.284°, 42.827°, 56.465°, 52.643°, and 62.734°. The peaks correspond to reflection planes (220), (311), (400), (511), (422), and (440), respectively. The X-ray diffraction showed the formation of Fe-phase in trivalent state and formation of FCC framework [51–54]. From the X-ray diffraction pattern, no additional reflection other than the FCC structure was found and this nullified the formation of any other phases unlike $NiFe_2O_4$ reported by Šepelák et al. [55] which exhibit additional reflections plane. The preferred orientation is found along (311) reflection plane. The multiple peaks show that the $ZnFe_2O_4$ sample is polycrystalline in nature. This result favorably agrees with experimental findings reported by Mahesh Chand et al. [57] and Akash Mishra et al. [56]. The crystallite size was examined via Small Angle X-ray Scattering (SAXS), Derby Scherrer, and Williamson–Hall method (W–H plot) using Eqs. (1) and (2), and the crystallite sizes obtained from these methods slightly vary from each other. Derby Scherrer was also used by Panahi-Kalamuei et al. [48] to examine the particle size of CeO_2 nanoparticles. The value of the lattice dislocation, lattice parameters, hopping length which is the distance between ions in the lattice, volume of the unit cell, and X-ray density of zinc ferrite sample were estimated using Eqs. (3) to (9) [66]

$$D = \frac{k\lambda}{\beta \cos\theta} \tag{1}$$

$$\beta_{hkl} \cos\theta = \frac{kh}{D} + 4 \in \sin\theta, \tag{2}$$

where k is constant factor, λ is the wavelength, β is the full width at half the maximum, D is crystallite size, and θ is the diffraction angle. The crystallite sizes obtained from Small Angle X-ray Scattering (SAXS), Derby Scherrer equation, and W–H plot are 12.32 nm, 9.47 nm, and 10.03 nm, respectively. The values of the lattice defects are 0.00487 $linm^{-2}$, 0.013939 $linm^{-2}$, and 0.007654 $linm^{-2}$, respectively

$$\delta = \frac{1}{D^2} \tag{3}$$

$$\sin^2\theta = \frac{\lambda^2}{3a^2}\left\{h^2 + k^2 + hk\right\} + \frac{\lambda^2 l^2}{4c^2} \tag{4}$$

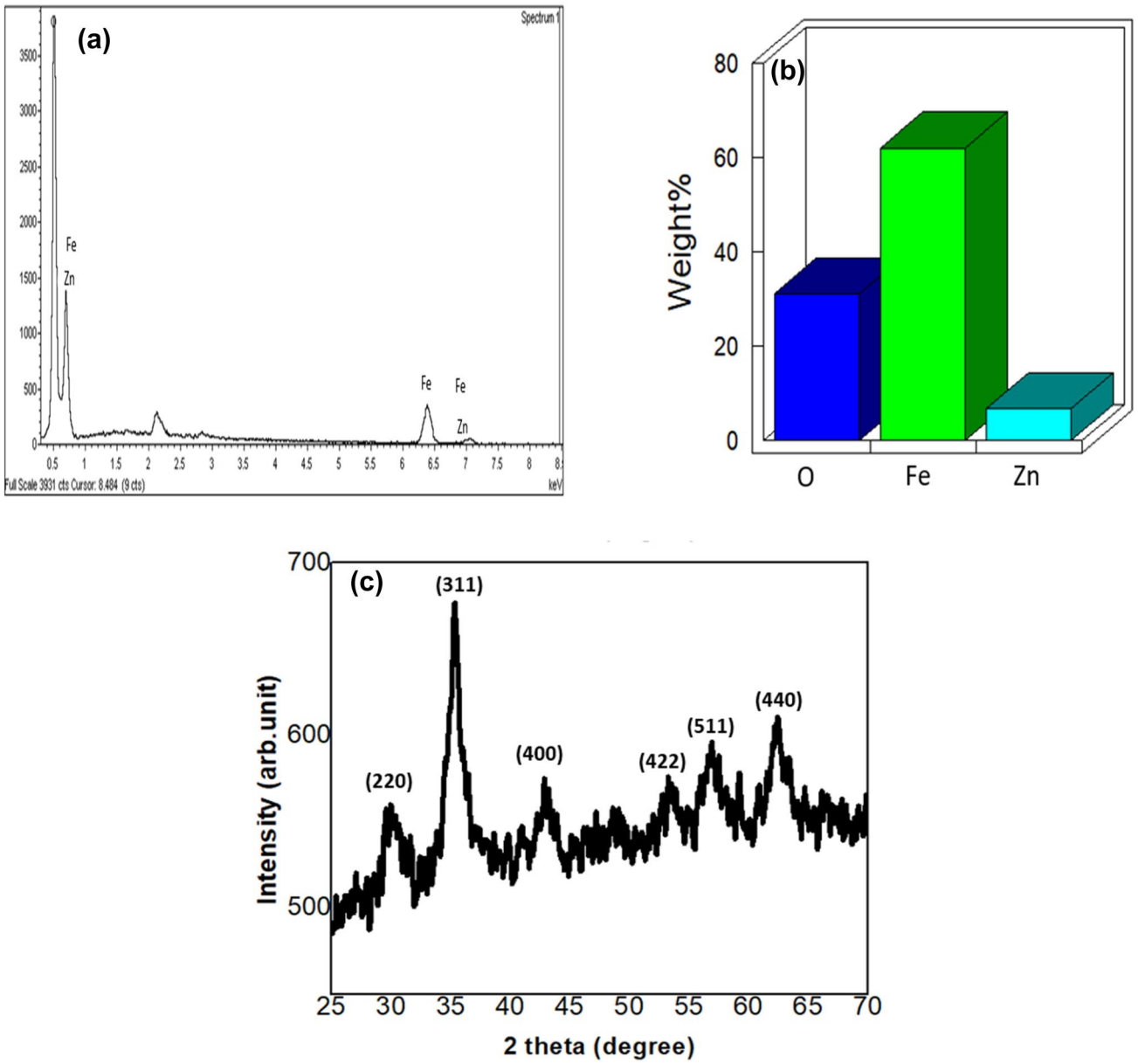

Fig. 2 Energy-dispersive X-ray and X-ray diffraction of $ZnFe_2O_4$ nanoparticles

$$L_{\mathrm{A}} = 0.25a\sqrt{3} \tag{5}$$

$$L_{\mathrm{B}} = 0.25a\sqrt{2} \tag{6}$$

$$\rho = \frac{1.66042\sum A}{V} \tag{7}$$

$$V = 0.866a^2c \tag{8}$$

$$\rho_x = \frac{8M}{N_{\mathrm{A}}a^3}, \tag{9}$$

where ΣA is the sum of atomic weights of the atoms in the unit cell, k is dimensionless shape factor, λ is the wavelength of X-ray, D is crystallite size, $\in$ is the micro-strain that occurred from the peak broadening, L_{A} is the hopping length in the tetrahedral site A, and L_{B} is the hopping length in the octahedral site B. The hopping lengths in the tetrahedral site A and octahedral site B are 3.61 nm and 2.94 nm. The lattice parameters a and c are 8.3298 Å and 13.7501 Å. The volume of the unit cell of the zinc ferrite nanoparticles is 239.653 $Å^3$, while the value of X-ray density is 5.2415 g/cm^3.

Scanning Electron Microscopy (SEM) technique was used to examine the surface structure parameters, such as surface morphology, surface porosity, grain shape, grain growth, presence of second-phase particles, and surface defect such as fracture. Similar technique was used by Gholami et al. [46] and Ghiyasiyan-Arania et al. [58], to examine the surface morphology of $NiAl_2O_4$/NiO nanocomposite and iron vanadate nanocomposite. The SEM image revealed a fairly porous morphology, showing that the particles are well compacted with negligible surface fracture, as shown in Fig. 3a. In addition, there is absence of surface defect such as cavity, pores, or hole. Few whitish particles were found, we assume the presence of the white traces on the surface to be Zn^{2+} ion particles, and this shows the mixing effect of zinc with ferrite. The morphology also reveals a closely packed structure, spheric-spongy shape with absence of second phase. The detailed studies of the Zinc ferrite microstructures were conducted, as shown in Fig. 3. The particle size is determined using the Transmission Electron Microscopy (TEM) image, as shown in Fig. 3b. The TEM showed that the particles are uniformly dispersed in the suspension, and this confirms the formation of stable nanofluid. Figure 3c shows the image obtained from HRTEM of ferrite sample which exhibit inter-planar spacing that corresponds to lattice reflection plane. The HRTEM image shows d-spacing of 0.27 nm which corresponds to (311) reflection planes. Information about the lattice spacing and atomic structure is revealed. The grain boundaries and interface from the HRTEM image were revealed. TEM image showed that the nanoparticle is made of small nano-diameter clusters of particles with formation of spherical shape.

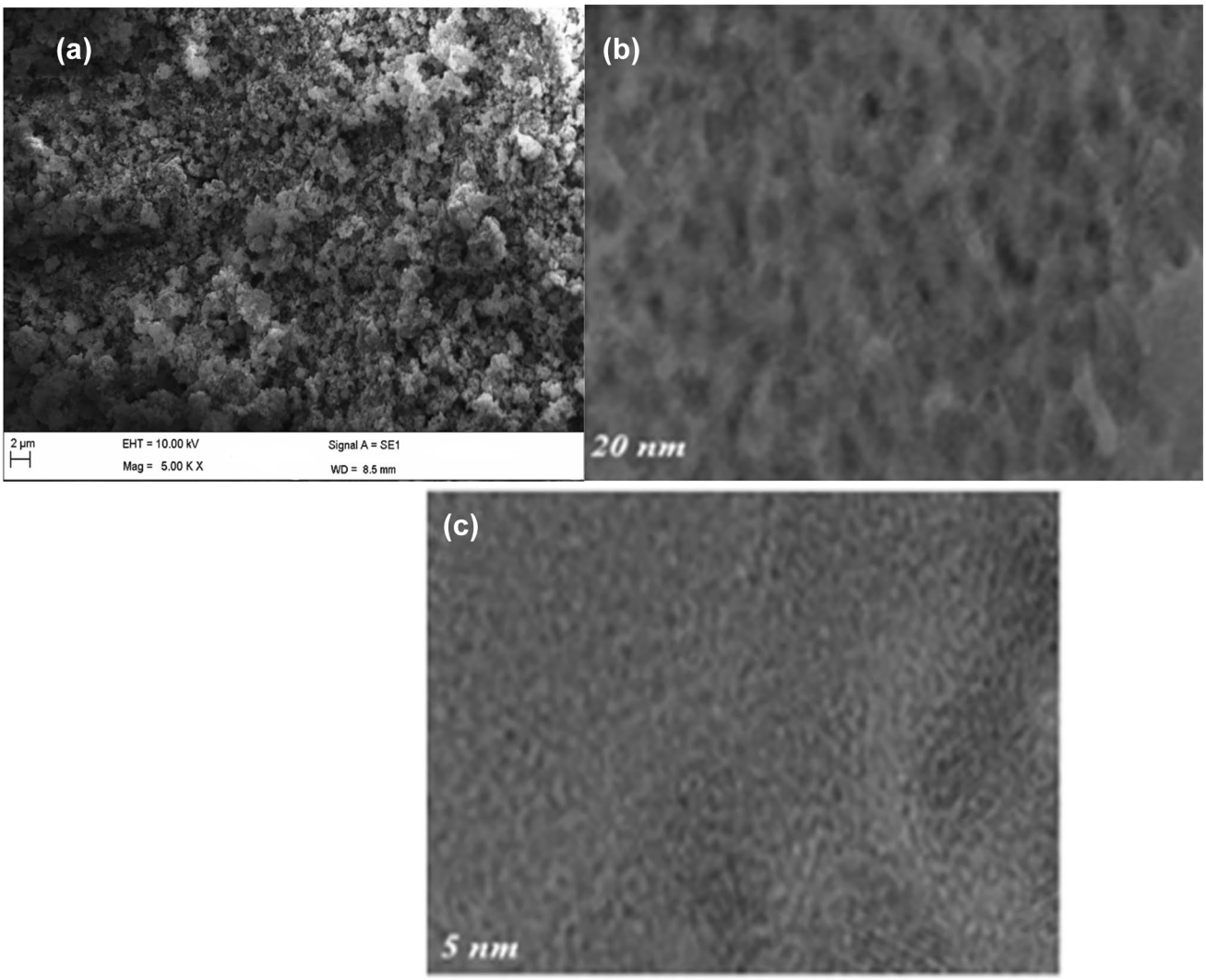

Fig. 3 **a** SEM image of $ZnFe_2O_4$ nanoparticles, **b** TEM, and **c** HRTEM of $ZnFe_2O_4$ magnetic nanoparticles

3.2 Photoluminescence and Fourier transform infrared spectroscopy of zinc ferrite magnetic nanoparticle

We used photoluminescence spectroscopy to examine the optical and luminescence effect of zinc ferrite particles. The luminescence property of the light emitted by the chemically synthesized $ZnFe_2O_4$ nanomagnetic samples is analyzed. The particle exhibits a very strong and narrow emission band at wavelength 565 nm with formation of yellow emission, as shown in Fig. 4a. This particle is typically useful in light emitting diode for the purpose of yellow emission. The sharp luminescence peak is attributed to the presence of a defect such as oxygen vacancies. The defect is due to donor levels that is close to the conduction band edge of the oxide [59]. The optical energy band gap of this compound was calculated using $1240/\lambda$, and it was evaluated as 2.21 eV. The FTIR spectra of the synthesized $ZnFe_2O_4$ nanomagnetic samples were used to examine the functional groups that are present in the compound and its composition. FTIR provides information on the basis of the chemical composition and physical state of the sample, and is very sensitive to changes in molecular structure. The FTIR spectral of the sample is represented in Fig. 4b. Strong absorption band is revealed around 1550/cm due to the presence of O–H-stretching vibration of the free or absorbed water, as shown in Fig. 4b. This confirms the presence of hydroxyl groups in $ZnFe_2O_4$ nanomagnetic samples [60]. The weak bands found around 1290 cm^{-1} are due to the formation of C=O-stretching vibration of the carboxylate group (CO^{2-}). The band formed around 950/cm is assigned to the formation of a no stretching vibration due to the existence of nitrate group [61–63]. The absorption bands formed at 580/cm and 670/cm are assigned to the existence of vibration of the tetrahedral and octahedral metal–oxygen (M–O) bonds in the lattices of the synthesized $ZnFe_2O_4$ nanomagnetic samples. The fairly strong absorption band found at 2450/cm is due to the formation of O=C=O-stretching vibration of carbonyl group which confirms the presence of carbon and oxygen in the ferrite compound.

3.3 Magnetic properties of zinc ferrite nanoparticles

The magnetic properties were examined using vibrating sample magnetometer (VSM). The magnetic elements such as saturation magnetization (M_S), remanence magnetization (M_r), coercivity (HC), and remanence ratio were obtained from hysteresis curve shown in Fig. 5. The applied magnetic field (H_c) is plotted against magnetization. From the curve, the value of the saturation magnetization is estimated to be 58.73 emu/g. The large saturation magnetization might be due to the crystalline nature of the nanoparticle and formation of minimum surface structure

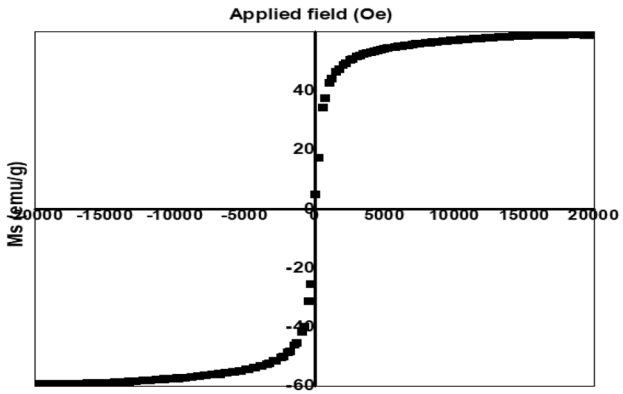

Fig. 5 Hysteresis loop of zinc ferrite nanofluid particle

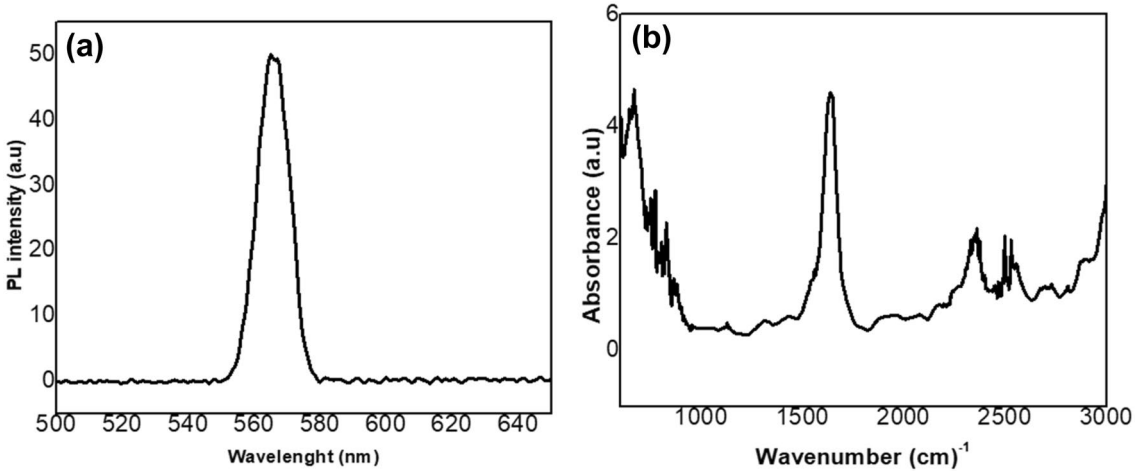

Fig. 4 **a** Photoluminescence (PL) and **b** FTIR spectroscopy of zinc ferrite magnetic nanoparticles

defect. The value of the remanent magnetization, coercivity, and remanence ratio are 5.05 emu/g, 29.54 Oe, and 0.3104, respectively. The remanence ratio is dependent on the saturation and remanence magnetization. The low coercivity indicates the formation of soft ferromagnetic and can be easily demagnetized. The high saturation magnetization is possibly due to small defects within the crystal lattice and low magnetic anisotropy which does not inhibit the magnetic moment alignment in the magnetic field. The magnetic hysteresis loop of zinc ferrite nanomagnetic particles revealed a superparamagnetic behavior. The low remanence magnetization of about 5.05 emu/g shows that the sample can simply retain low proper magnetism and is said to be soft magnetic. The magnetization M of superparamagnetic particles can be shown as [56, 57]

$$M = \int_0^\infty L(\alpha) f(D) d(D) \tag{10}$$

$$\text{where } L(\alpha)\text{is the Langevin function} = L(\alpha) = M_s^f \left(\cot h(\alpha) - \frac{1}{(\alpha)} \right) \tag{11}$$

$$\text{But } M_s^f = M_d \emptyset \text{ and } \alpha = M_d H \frac{(1/6)\pi D^3}{K_b T}.$$

$f(D)$ is log-normal size distribution, H is applied magnetic field, k is the Boltzmann constant, T is temperature, M_s^f is fluid magnetization, $\emptyset$ is solid volume fraction, and M_d is domain magnetization. The particle diameter (D_m) is 7.03 nm, domain magnetization (M_d) is 159 G, and a solid volume fraction of 0.0057 was obtained.

The magnetic curve revealed a superparamagnetic effect alongside low coercivity (Hc). The superparamagnetic is attributed to small crystallite size of the nanomagnetic particle. This effect makes zinc ferrite nanomagnetic particles to be thermally activated to overcome magnetic anisotropy [64]. The required minimum volume of particles needed to acquire superparamagnetic behavior is calculated from the equation [64]

$$V_p = 25 k_B \frac{T}{K}, \tag{12}$$

where k_B is Boltzmann constant, k is anisotropy constant, and T is temperature. Thus, the size of the synthesized cobalt spinel ferrite nanomagnetic particle is less than 10 nm which is below the critical size limit that shows superparamagnetic nature. The magneton number of the sample was calculated using equation [64]

$$n_B = \frac{M_w \times M_s}{5585}, \tag{13}$$

where M_w is the molecular weight and M_s is the saturation magnetization. The magnetic behavior of the sample was examined using Neel's model. By Neel's model two-sublattice model, the magnetic moment n_B is expressed as [64]

$$n_B = M_B - M_A, \tag{14}$$

where M_B and M_A are the magnetic moments of B-site and A-site. Neel's magnetic moment was examined using the cation distribution obtained from X-ray diffraction analysis. We observed differences in calculated values of magnetic moment and observed magnetic moment. This suggests the possibility of canted spin. The existing canted spin and magnetic moment behavior were obtained using the Yafet–Kittel angle (α_{Y-K}). The Yafet–Kittel angle (α_{Y-K}) was examined using the equation below [65, 66]

$$\alpha_{Y-K} = \cos^{-1} \frac{n_B - M_A}{M_B}. \tag{15}$$

The calculated Y–K angle is 38.72 (degree). Since the Y–K angle is not zero, it suggests that the canted spin model of magnetization is fit on the B-site and this results to the decrease in A–B interaction and enhanced B–B interaction [56]. Particle–particle interaction is examined using a coupling constant (λ). The coupling constant is the ratio of the magnetic dipole interaction energy between two coated particles in contact with their thermal energy. It gives information about the strength of particles interaction and estimates the typical force exerted when the nanoparticles are interacting. The coupling constant is estimated using $\lambda = \frac{m^2}{d_h^3 K_B T}$ [57], where m is the mass of the particle, k_B is Boltzmann constant, k is anisotropy constant, and T is temperature. A coupling constant of 2.06 is formed, since the value of the coupling constant is greater than one, and strong inter-particle interactions are formed. The chain-like structure is strong enough to overpower the thermal reaction; this occurred only when coupling constant is greater than one [56].

3.4 Rheological properties

3.4.1 Complex magneto-viscous effect

Strain amplitude sweep test was carried out for zinc ferrite nanomagnetic fluid in the absence and presence of magnetic fields. The complex magnetoviscosity is examined at strain amplitudes 1%, 10%, 33%, and 100%, respectively. Maximum complex viscosity is formed when strain rate 1% is applied in the presence of magnetic field, this implies that at strain rate 1%, the fluid becomes hardened, and fluid flow is restricted from free flow. In the absence of magnetic field,

the nanofluid shows minimum complex viscous effect; this occurred, because field-induced structure does not form. The particle suspensions exhibit a relatively low viscous effect in the absence of magnetic field due to absence of particle magnetization. In the presence of magnetic field, the particles are magnetized and interact with one another along the direction of the magnetic field. It is seen from Fig. 6 that complex viscosity is decreased with increasing strain rate. At low strain application and presence of magnetic field, enhanced magnetically field-induced structures were formed, the magnetically induced structure is more enhanced as the applied magnetic field is increased, and this results in the formation of increasing complex viscosity. But upon increasing the strain rate, the complex viscosity is decreased and the resistance to fluid flow is reduced, and this results in the frustration of hardening effect of the fluid. This occurred, because the field-induced chains break down and the field-induced structure is destroyed. Result shows that at low strain application, the fluid particles are orderly arranged when magnetic field is applied, but when the strain rate is increased, particles are randomly dispersed in fluid, and their orientations are formed along the direction of shear, this leads to decrease in complex viscosity. This implies that the field-induced structure is sustained at low strain application, whereas at high strain amplitude, the particle orientation is frustrated and the magnetic structures are destroyed [52, 66–68].

Result shows that complex viscosity is increased with increasing magnetic field due to enhanced dipolar interaction and the formation of enhanced magnetically induced

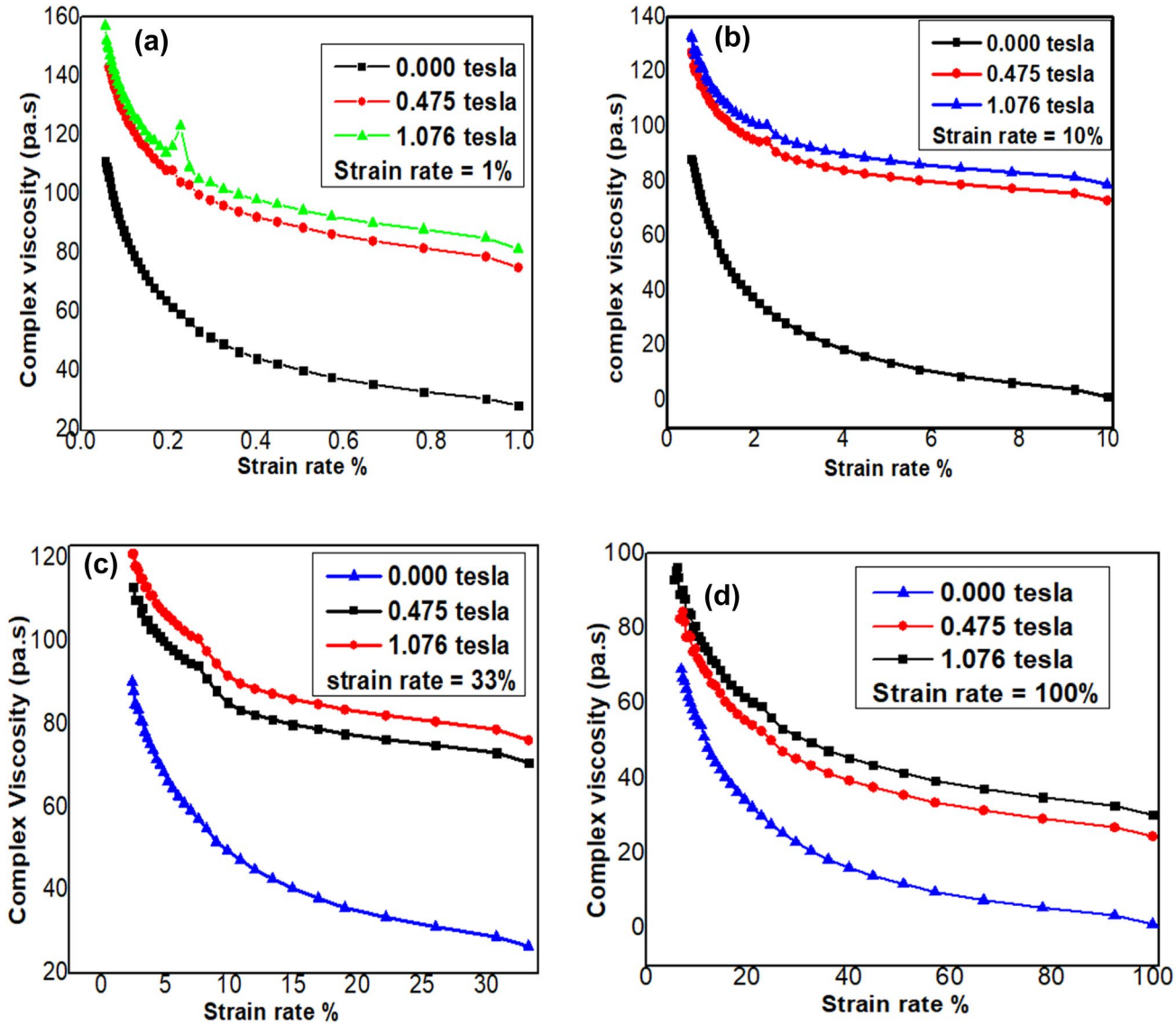

Fig. 6 Complex viscosity against strain amplitude of $ZnFe_2O_4$ nanofluid at strain: **a** 1%, **b** 10%, **c** 33%, and **d** 100%

chain structures. Formation of long chains in the direction of the magnetic field is revealed at low strain application, and the long chain limits the fluid flow due to high complex viscosity. However, at high strain application, the long chain breaks and the complex viscosity is decreased. Alternatively, literature has revealed that the viscous effect of fluid can be minimized by mixing the fluid particles with particles of carbon nanotube. Recent report by Leona et al. [69], showed that if fluid particle is mixed with particle of carbon nanotube, the viscous effect will be minimized; this is formed, because the induced structure of the fluid particle breaks down; and the dipolar interaction of the magnetic nanoparticles is frustrated.

Varying fluid flows were formed at strain 1%, 10%, 33%, and 100%, and this illustrates the formation of fluid flow-dependency of zinc ferrite magnetic fluid on the strain rate. From indication, at 1% strain application and in the presence of magnetic field 1.076 T, solid-like and elastic fluid is formed and the fluid flow is not free; this occurred due to formation of large elastic structure, high complex viscosity, and high resistance to fluid flow. High resistance to fluid flow is formed, because the low strain application is not susceptible of resisting the magnetostatic force; henceforth, the strain cannot impair the particle aggregates. The particles are henceforth strongly bound to the aggregates due to prevailing magnetostatic force. Result show that the magnetostatic interaction of the dipoles in the magnetic realm is prevalent over the strain effect, and this leads to formation of substantial aggregate. The resistance to fluid flow slightly decreases when the applied magnetic field is reduced to 0.475 T, and a semi-elastic fluid is formed. We cannot absolutely say that the decrease in resistance to fluid flow is due to low strain application alone, but as a result of combine effect of diminished magnetostatic force. The weak magnetostatic force gives low strain application the chances to slightly deform the magnetic structure, whereas strong magnetostatic force does not give low strain the chance of destroying the magnetic structure. The fluid flow furtherly diminishes when magnetic field is absent; this occurred, because the magnetostatic force has been withdrawn.

In the presence of magnetic field 1.076 T and strain10% and 33%, the resistance to fluid flow is low compared with resistance to fluid flow formed under 1% strain; despite the same magnetic force is applied, this occurred due to rise in the magnitude of the deformation formed by strain 10% and 33%. Resistance to fluid flow is decreased, because the intermediate strain applications are susceptible of partially destroying the magnetic fluid structure; this shows that the intermediate strain 10% and 33% are partially resistible over the magnetostatic force. Result shows that the magnetostatic interaction of the dipoles in the magnetic domain is not capable of fully resisting 33% strain, the magnetic structure is henceforth partially destroy and the fluid becomes softened, and this results to decrease in complex magnetoviscosity. From indication, the intermediate strain applications partially deformed the magnetic aggregates, this segregates certain fraction of the particles from their respective aggregates, and the segregated particles are henceforth become individual. This illustration explains one of the factors responsible for decrease in complex viscosity and formation of weaken resistance to fluid flow as the strain rate is increased. Slight decrease in resistance to fluid flow is formed when the applied magnetic field is decreased to 0.475 T. This is formed due to weaken magnetostatic force which diminishes the dipolar interaction of the magnetic dipoles in the magnetic domain. In the absence of magnetic field, the magnetostatic interaction of the dipoles is completely destroyed, and this disrupts the chains connecting the particles. The absence of magnetostatic force allows the strain to fully deform the magnetic structure; henceforth, the complex viscosity is hugely diminished and the resistance to fluid flow is largely frustrated.

At 100% strain application and in the presence of magnetic field 1.076 T, the magnetic structure is extensively deformed, and this is formed due to high strain application which extensively destroys the magnetic aggregates. The destruction of the magnetic aggregate leads to formation of extremely low complex magnetoviscosity and extremely weakened resistance to fluid flow; this is formed due to high strain application which is extensively susceptible of frustrating the magnetic dipoles interaction. The destruction of the magnetic structure by high strain largely weakened the magnetostatic force. Result shows that the magnetostatic interaction of the magnetic dipoles cannot resist high strain effect, and this leads to huge deformation of the magnetic aggregates. The resistance to fluid flow is decreased when the applied magnetic field is decreased to 0.475 T; this occurred due to decrease in magnetostatic force effect. The magnetic aggregate is largely deformed due to combine effect of weaken magnetostatic forces and high strain application. The low interaction of the magnetic dipoles cannot adequately resist large deformation caused by high strain. The low magnetostatic force allows the high strain to wholly deform the microstructure of the fluid aggregates. Very huge decrease in complex magnetoviscosity is recorded in the absence of magnetic field; this occurred, because the magnetostatic force is either extremely weakened or completely removed.

The complex viscosity is increased with increasing strength of the magnetic field as a result of dipole–dipole interaction and formation of field-induced chain-like structures in the direction of the magnetic field. Dipole moment of a magnetic nanoparticle is given by $\mu = V\chi H$ [4], where v is the volume of the nanoparticle and is related by $V = \frac{\pi d^3}{6}$ [4], χ is the magnetic susceptibility of the particle, and H is the applied magnetic field. There is formation of long

chains by high magnetic field application [70], the long chain restricts the fluid flow, and this results in the formation of increasing complex viscosity. Brownian dispersion provides opposition to the formation of particle aggregates, and the Brownian dispersion against field-induced aggregation can be illustrated using coupling constant [4]

$$\lambda = \frac{\pi(\mu_o \chi H)^2 d^3}{6k_B T},$$

where μ_o is the permeability of free space and H is applied magnetic field, respectively, T is the absolute temperature, and K_B is Boltzmann constant. If $\lambda \gg 1$, the particle aggregation is strongly promoted [71], but if $\lambda \ll 1$, dispersion is promoted; this is a useful parameter that can be used during the design of ferrofluid [72]. If there is formation of micrometer-sized magnetic particles in the ferrofluid, the aggregation parameter can be calculated for a nanometer-sized magnetite sphere using the below equation, but our particle is in nanometer-sized [73]

$$\lambda = \frac{\mu_o M_s H \pi d^3}{18k_B T},$$

where $\mu_o M_s$ is the saturation magnetization of the particles. The coupling parameter λ is important factor that reveals the equilibrium suspension of the chain structures of the magnetic nanoparticles. The magnitude of λ for micron-sized particles is higher (~ 95.4) [73] as compared to nanometer-sized particles (~ 1.3); this shows that the dipolar interaction from different particle size particles is a crucial yardstick in the formation of cluster.

3.4.2 Storage and loss modulus

Strain amplitude sweep test in oscillatory mode is used to examine the viscoelastic behavior of zinc ferrite ferrofluid.

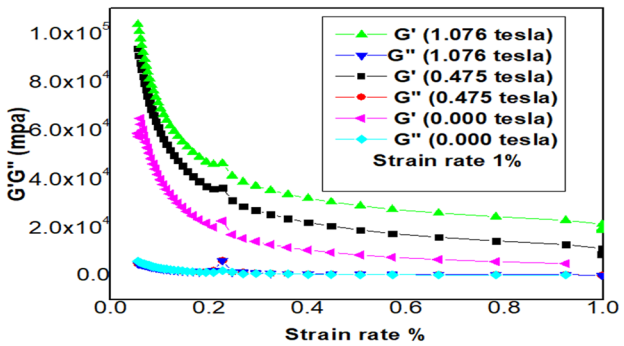

Fig. 7 Storage modulus (G') and loss modulus (G'') against strain amplitude of $ZnFe_2O_4$ nanofluid at strain rate 1% in the absence of magnetic field (0.000 T) and presence of magnetic field 0.475 T and 1.076 T

The influence of strain application on storage modulus and loss modulus in the presence and absence of magnetic field is accurately examined, and the results are illustrated, as shown in Figs. 7, 8, 9, and 10. The strain amplitude test was performed under strain amplitude 1%, 10%, 33%, and 100%, respectively. At low strain amplitude, the storage or elastic modulus (G') is far greater than the loss or viscous modulus (G'') of the ferrofluid. The storage modulus is an important parameter which determines the energy storage capacity and elastic structure of the viscoelastic system, whereas the loss modulus determines the rate at which energy is loss or dissipated and the viscous nature of the system. Nonlinear viscoelastic is formed within low strain rate region; at this region, a non-Newtonian behavior is established and the elastic modulus is far greater than the loss modulus; this

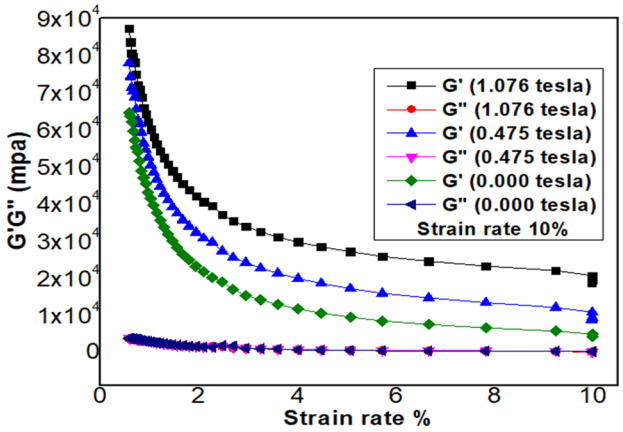

Fig. 8 Storage modulus (G') and loss modulus (G'') against strain amplitude of $ZnFe_2O_4$ nanofluid at strain rate 10% in the absence of magnetic field (0.000 T) and presence of magnetic field 0.475 T and 1.076 T

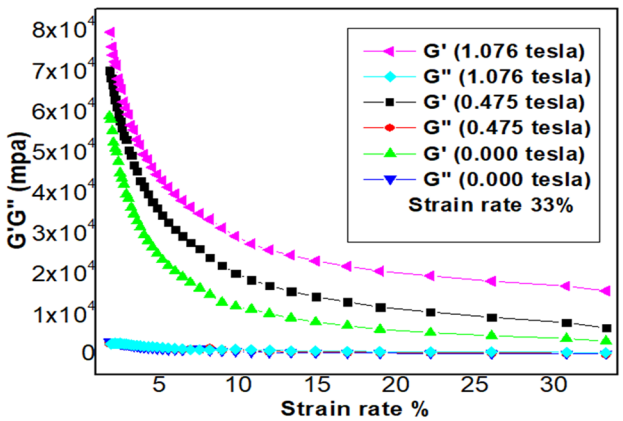

Fig. 9 Storage modulus (G') and loss modulus (G'') against strain amplitude of $ZnFe_2O_4$ nanofluid at strain rate 33% in the absence of magnetic field (0.000 T) and presence of magnetic field 0.475 T and 1.076 T

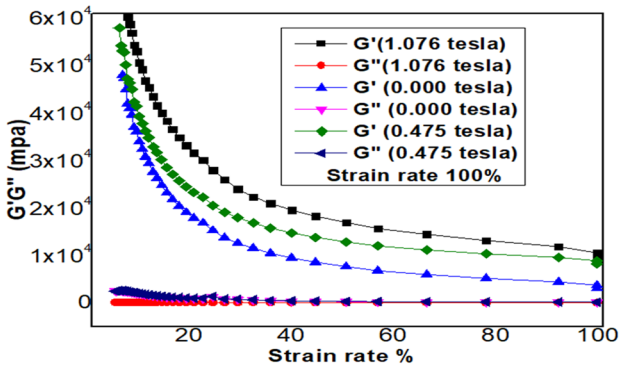

Fig. 10 Storage modulus (G') and loss modulus (G'') against strain amplitude of $ZnFe_2O_4$ nanofluid at strain amplitude 100% in the **a** absence of magnetic field (0.000 T) and presence of magnetic field **b** 0.475 T and **c** 1.076 T

shows that the viscoelastic system is being dominated by elastic structure; this occurred, because magnetostatic forces is dominant over hydrodynamic forces. The result revealed the formation of a super elastic structure due to extremely high storage modulus of maximum value of order 10^5 and low-loss modulus of maximum value of order 10^2. The result indicates the existence of stronger elastic links between the magnetic nanoparticles that create microscopic structure of the suspensions at low strain application [74]. The increase in strain slightly diminished the field-induced elastic structure, and the solid-like structure is henceforth sustained over a wide range of strain application. The absence of crossover between G' and G'' indicates that no transition from solid to liquid-like behavior was formed. The result revealed the formation of improved energy storage capacity when strain rate 1% is applied, and the energy storage capacity is decreased with increasing strain rate.

Various viscoelastic responses were formed at strain amplitudes 1%, 10%, 33%, and 100%, and this illustrates the dependent of microstructural deformation of zinc ferrite magnetic structure on the strain percentage. From indications, at strain 1% and in the presence of 1.076 T, structural deformation is low, and this supports the formation of enhanced elastic structure with maximum value of the order 10^5. Enhanced viscoelastic system is formed, because the low strain application is not susceptible of destroying the chains connecting the particles; henceforth, the particles are strongly attached to the aggregate due to prevalent magnetostatic force. The magnetostatic interaction of the dipoles in the magnetic realm is resistant over the strain effect due to formation of large elastic structure. The formation of high elastic structure is suitable for designing a system that can accommodate huge energy storage capacity. Large energy can be stored due to formation of low-loss modulus which prevents the system from dissipating much energy. The viscoelastic response and energy storage capacity are slightly decreased when the applied magnetic field is lowered to 0.475 T. The viscoelastic quantity is decreased to maximum value of 9×10^4 which is still very closer to viscoelastic response of the order 10^5 obtained at 1.076 T. We cannot actually say that the decrease in viscoelastic response is due to strain effect alone, but also due to effect of weak magnetostatic force. At 0.475 T, the magnetostatic force effect is weakened, and the weak magnetostatic force gives low strain effect the chances to deform the magnetic structure. This occurred, because the low magnetostatic force is not fully capable of resisting the strain effect; henceforth, the formation of diminished elastic structure and reduced energy storage capacity is revealed. Large decrease in the viscoelastic response is formed in the absence of magnetic field; this occurred, because the magnetostatic force is extremely weaken or completely withdrawn. The order of the loss modulus is 10^2, this value is lower as compared with order 10^5 for storage modulus, and this illustrates the formation of dominant magnetostatic force over hydrodynamic force.

At intermediate strain 10% and 33% applications and in the presence of magnetic field 1.076 T, the deformation provided by the strain applications is higher compared with deformation provided by strain 1% despite the same magnetic influence. Decrease in viscoelastic response is formed, because increasing strain to 10% and 33% partially destroys the fluid structure, the structures are deformed only in small magnitude, and this demonstrates strain 10% and 33% as been partially resistant over the magnetostatic force. This occurred, because the magnetostatic interaction of the dipoles in the magnetic domain is not utmostly resistant over the strain effect. The energy storage capacity also decreases in small magnitude due to partial destruction of the elastic structure. The viscoelastic response decreases slightly when the applied magnetic field is lowered to 0.475 T. When magnetic field is reduced, the magnetic dipole interaction is weakened, and this gives the strain effect the ability to be resistant over the magnetostatic force. This effect leads to the disruption of chains that connect the particles. Large deformation of the elastic structure is formed in the absence of magnetic field, and this occurred due to drastic weakening of the magnetostatic force.

At 100% strain application and in the presence of magnetic field 1.076 T, the magnetic structure is largely deformed; this occurred due to high strain application that is susceptible of weakening the magnetostatic force. The deformation formed under the strain 100% is higher compared with deformation formed under strain 10% despite the application of same magnetic field. The magnetic structure is extremely destroyed at very high strain, and this segregates the particles from the aggregate due to weakened magnetostatic force. This occurred, because the magnetostatic interaction of the magnetic dipoles is not resistant over the strain effect; henceforth, larger fraction of the magnetic structure is

deformed. The structure is deformed, because the weak magnetostatic force is not resistant over the high strain effect; henceforth, the elastic structure is destroyed. The viscoelastic response is decreased when the applied magnetic field is decreased to 0.475 T. Large decrease in the viscoelastic value is recorded in the absence of magnetic field; this occurred, because the magnetostatic force is extremely weak or even completely removed.

Our result agrees with experimental findings reported by Mahesh et al. [75] who reported zero-phase transition across all strains. The loss modulus is actually not influenced by varying the strain amplitude; this is due to the formation of linear viscoelastic behavior [76, 77]. The value of the storage modulus ranges between 2500 pa and 100,000 pa which is about 33 times more than the values obtained in previous work reported by Yu Tong et al. and other researchers [56, 57, 79], and this supports the formation of super elastic behavior and enhanced energy storage capacity. At 1% strain application, the viscoelastic performance is largely improved with dominant elastic nature when magnetic field is applied; whereas, when magnetic field is withdrawn, diminished viscoelastic performance is formed. This effect is reversed when 100% strain is applied. Solid-like behavior is dominated both in the absence and presence of magnetic field at all strain applications, but Leona and John Philip reported pure liquid-like ferrofluid when magnetic field was not applied [7, 69]. Enhanced viscoelastic that exhibits elastic structure of the order 10^5 and about five times greater than value reported by Balaji et al., and extremely greater than value reported by Chattopadhyay is established [78]. Balaji et al. also reported increase in storage and loss modulus with increasing angular frequency. Yongbo et al. obtained experimental results which is accurately in agreement with our findings report, because the research team reported storage modulus which is far greater than loss modulus as we also did. Yongbo et al. also reported the formation of elastic dominant structure and solid-like nanofluid alongside the formation of phase transition at high strain amplitude [75]. Dependency of elastic modulus on strain rate was established by Mitsumata and Okazaki and the elastic modulus is decreased with increasing strain [6] which accurately accords with our work.

3.4.3 Torque of zinc ferrofluid

Figure 11a–c shows the transmitting torque of zinc ferrite ferrofluid at strain application 1%, 10%, and 33%, respectively. The effect of strain rates on the transmitting torque is examined both in the absence and presence of magnetic fields. We see from the result that the transmitting torque is increased with increasing strain rate. Low transmitting torque is formed under the application of magnetic field and strain rate 1%, and this leads to the formation of low rotation of the fluid particles. The low transmitting torque slowly rotates the magnetic field in a manner that cannot destroy the field-induced structure, and this supports the formation of enhanced magneto-viscous effect. At magnetic field 1.076 T and strain rate 1%, low torque is formed, and the torque is decreased when the magnetic field is reduced to 0.475 T. In the absence of magnetic field, drastic decrease in torque is revealed. Low torque is formed by low strain application, it means that the magnetic field is slowly rotated, and the slow rotation cannot destroy the rotating magnetic field. Since the magnetic field is not destroyed, it shows that the magnetostatic force cannot be destroyed by the rotating effect of the magnetic field; this supports the formation of high magnetoviscosity under the application of 1% strain. When the strain is increased to 10%, the torque is increased, and higher torque is formed under the application of 1.076 T, but when magnetic field is decreased to 0.475 T, the torque is reduced. The rotation of the magnetic field is increased at 10% strain and is higher compared with rotation formed under 1% strain. The rotating magnetic field cannot utmostly resist the rotating force provide by 10% strain application; henceforth, the magnetic field is partially destroyed by the rotating effect. When the magnetic field is withdrawn, the torque is decreased further. Increasing strain to 10% partially increases the torque and the rotation of the rotating magnetic field, and this partially destroys the magnetic field. This destruction weakened the magnetostatic force which results to the partial destruction of the magnetic aggregate. This accounts for one of the reasons reduced magnetoviscosity is formed under 10% strain as compared with magnetoviscosity formed under 1% strain application. When 33% strain is applied, maximum dynamic rotation is formed due to high transmitting torque, and this leads to the formation of high rotation of magnetic field. Due to highly rotating magnetic field, the field-induced structure and the particle aggregates are extremely destroyed, and this leads to the formation of low magneto-viscous effect. Zinc ferrite formed enhanced viscoelastic effect due to formation of low transmitting torque, whereas the viscoelastic effect is diminished when high strain application is used due to highly rotating magnetic field. This experimental evidence is attributed to magnetization of the induced magnetic structure of the suspended nanoparticles. The presence of magnetic field caused the attraction of the magnetic nanoparticle due to magnetization by the magnetic flux and formed anisometric aggregates which could be either destroyed or preserve in the presence of respective strain rate.

Due to nanometer size of the particles, the particle interaction is affected by Brownian motion, and certain amount of energy is henceforth needed to overcome the Brownian motion of the magnetic nanoparticles to form a chain-like structure and particle aggregate. The Brownian motion is overcome by low strain application and low transmitting

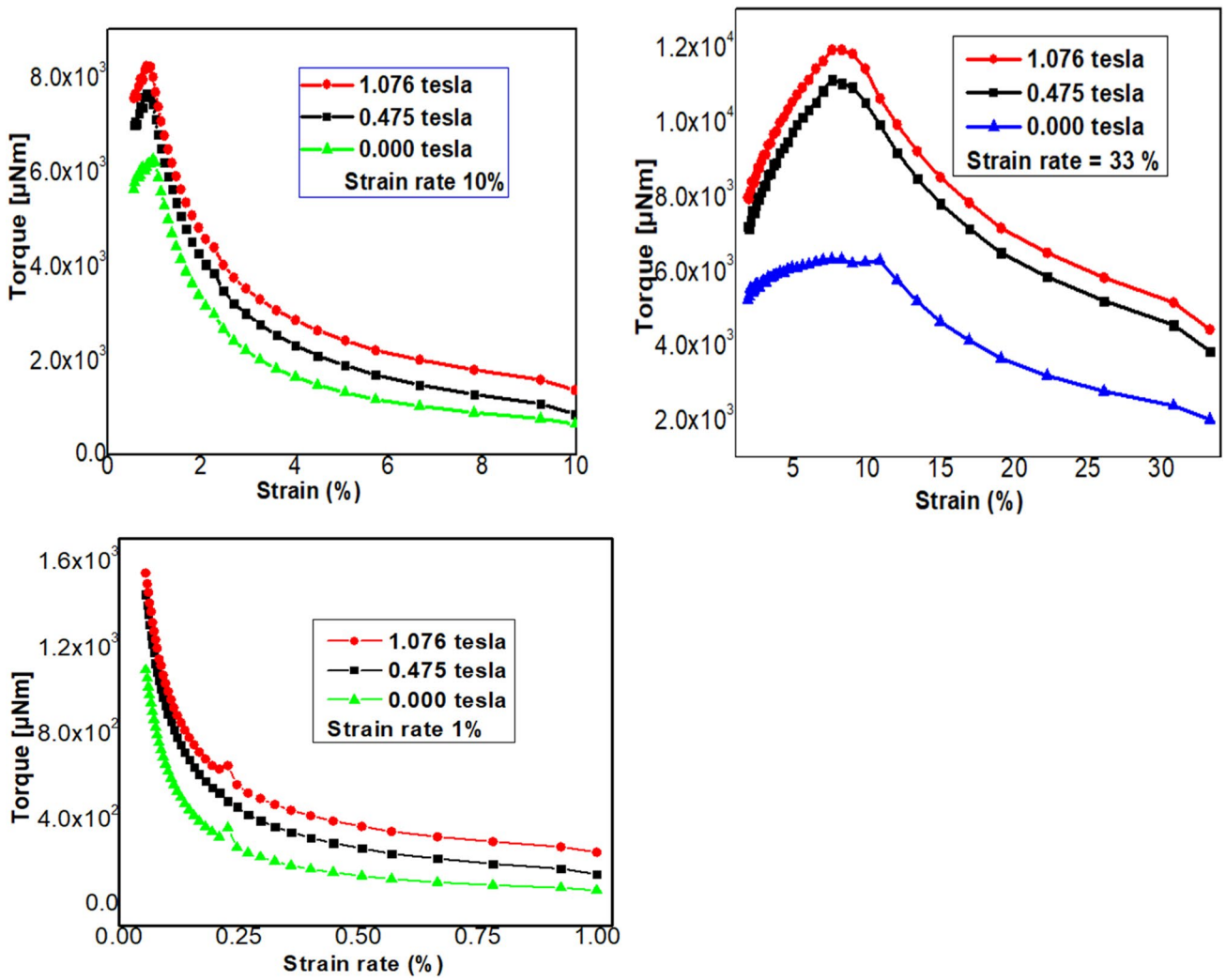

Fig. 11 Torque of $ZnFe_2O_4$ magnetic nanofluid at strain rate 1%, 10%, and 33%

torque which support the formation of aggregate, and the formation of aggregate is assisted by slowly rotating magnetic field. The field-induced structure is enhanced due to formation of low torque [75]. For sufficiently large values of transmitting torque, high strain application is required, whereas for sufficiently low transmitting torque, low strain application is required. Magnetostatic particle interactions are dominated over thermal motion which result in the formation of enhanced chain-like particle aggregates at low strain and low transmitting torque. However, at high strain and high transmitting torque, the thermal motion is dominated over magnetostatic particle interactions, and this results in the formation of frustrated chain-like particle aggregates. Brownian motion is also dominated and field-induced aggregates are damaged, but Brownian motion is not dominated at low strain application.

3.4.4 Relaxation modulus

The dependency of relaxation modulus of zinc ferrite ferrofluid on time interval is illustrated in Fig. 12. Result shows

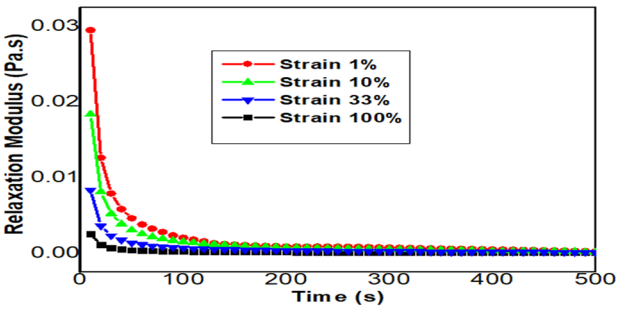

Fig. 12 Relaxation modulus against strain rate of $ZnFe_2O_4$ nanofluid at strain rate 1%, 10%, 33%, and 100%

that rheological system can be progressively preserved if the imposed shear stress relaxes at a particular time interval. If imposed shear stress is not controlled and critical stress is reached, the viscoelastic properties will be totally deformed and the system will be dominated by plastic features due to deformation of elastic properties. The viscoelastic system can be prevented from deformation by applying appropriate relaxation modulus, and this relaxes the imposed stress and returns the system to equilibrium state where a steady-state flow is formed. Study shows that the imposed shear stress needs to be relaxed to return the rheological system to its equilibrium state after when it has sheared. Several studies revealed that if the rheological system is not allowed or forced to be relaxed, the system will be perturbed and rheological properties of the system will be destroyed [80]. Result shows that relaxation modulus is decreased rapidly with increasing time between time interval up to 30 s when a steady state begins to form. A non-steady-state flow is formed at the time interval before 30 s. At relaxation time beyond 30 s, stress relaxation remains constant; this indicates the formation of a steady-state flow. The formation of large relaxation modulus is established when high strain rate 100% is involved. The application of suitable relaxation modulus prevents the rheological system from any kind of deformation. Relaxation modulus of zinc ferrite ferrofluid is reported for the first time to the best of our knowledge, and the condition required for the formation of steady-state flow is established. Result shows that the relaxation modulus decreases with increasing strain rate. The rheological system is sustained via the application of appropriate relaxation modulus that can sufficiently frustrate the imposed stress; this allows the formation of a steady-state flow. This steady-state flow was obtained at a time interval beyond 30 s where a linear relaxation is attained and showed a Newtonian behavior. Through linear relaxation, the imposed stress could not allow any structural reformation or rearrangement. The existing linear relaxation is attributed to the formation of linear chains structure and densely packed bulk aggregates [81]. The highest value of relaxation modulus is revealed by 1% strain application, whereas 100% strain revealed the lowest relaxation modulus.

3.4.5 Shear stress against strain amplitude of zinc ferrite nanofluid

Figure 13a–d depicts the graphs of shear stress against strain 1%, 10%, 33%, and 100% in the absence and presence of magnetic fields. At low strain rate, low shear stress is formed; this results in the formation of high magnetoviscosity; this occurred, because low shear stress cannot break the field-induced structures; the chain joining the particles and the particle aggregates are henceforth preserved. This effect leads to the formation of high resistance to fluid flow and high complex magnetoviscosity. Result shows that the shear stress is increased with increasing strain rate as indicated in Fig. 13. When high strain rate is applied, high shear stress is formed, the high stress breaks the field-induced structure and destroyed the particle aggregates, and this results in the formation of decreasing complex magnetoviscosity which stops the restriction to fluid flow.

From indication, at 1% strain application and in the presence of magnetic field 1.076 T, low shear stress is formed. Result show that the low shear stress is not resistible over the effect of the magnetostatic force, this makes the low stress not to be susceptible of breaking the magnetic structures; this observation accounts for one of the reasons; high magnetoviscosity is formed under 1% strain application as discussed in the previous sections. It is generally noted that large aggregate with strongly bounded with particles is required for the formation of high magnetoviscosity. The magnetoviscosity will be reduced if the particles are segregated from the aggregate. The particles can be segregated from the aggregate only with the effect of larger shear stress. Since 1% strain forms smaller shear stress, henceforth, the low stress cannot resist the magnetic forces binding the particles to the aggregate. Since the particles cannot be segregated by small stress under the application of 1% strain, the magnetic structure is henceforth sustained and enhanced magnetoviscosity is formed. The shear stress slightly decreases when the applied magnetic field is reduced to 0.475 T. Further decrease in shear stress is formed when magnetic field is withdrawn. At strain rate 10%, increasing shear stress is formed. The shear stress increases from maximum stress 600 pa formed under 1% strain to maximum stress 6000 pa formed under 10% strain at high strain rate regions. The formation of increasing stress from 1 to 10% strain leads to destruction of only certain fraction of the magnetic structure; this show that at 10% strain, the magnetostatic force is not utmostly capable of being resistant over the shear force. Result shows that the shear force is just partially resistible to the magnetostatic force, it henceforth partially weakens the magnetic forces binding the particle to the aggregates, and the particles are thus segregated only in small magnitude. The destruction of the aggregate leads to formation of decreasing magnetoviscosity. The shear stress is increased under the application of 1.076 T at 10% strain, and the shear force is decreased when the magnetic field is decreased to 0.475 T and when it is withdrawn. Result shows that at 33% strain, higher shear stress is formed; the formation of the larger shear force utmostly breaks down the magnetic structure; this occurred, because the magnetostatic force is not capable of resisting the effect of the shear force. Result shows that the shear force is largely resistant over the magnetostatic force at 33% strain; this frustrates and weakens the magnetic force binding the particle to the aggregates;

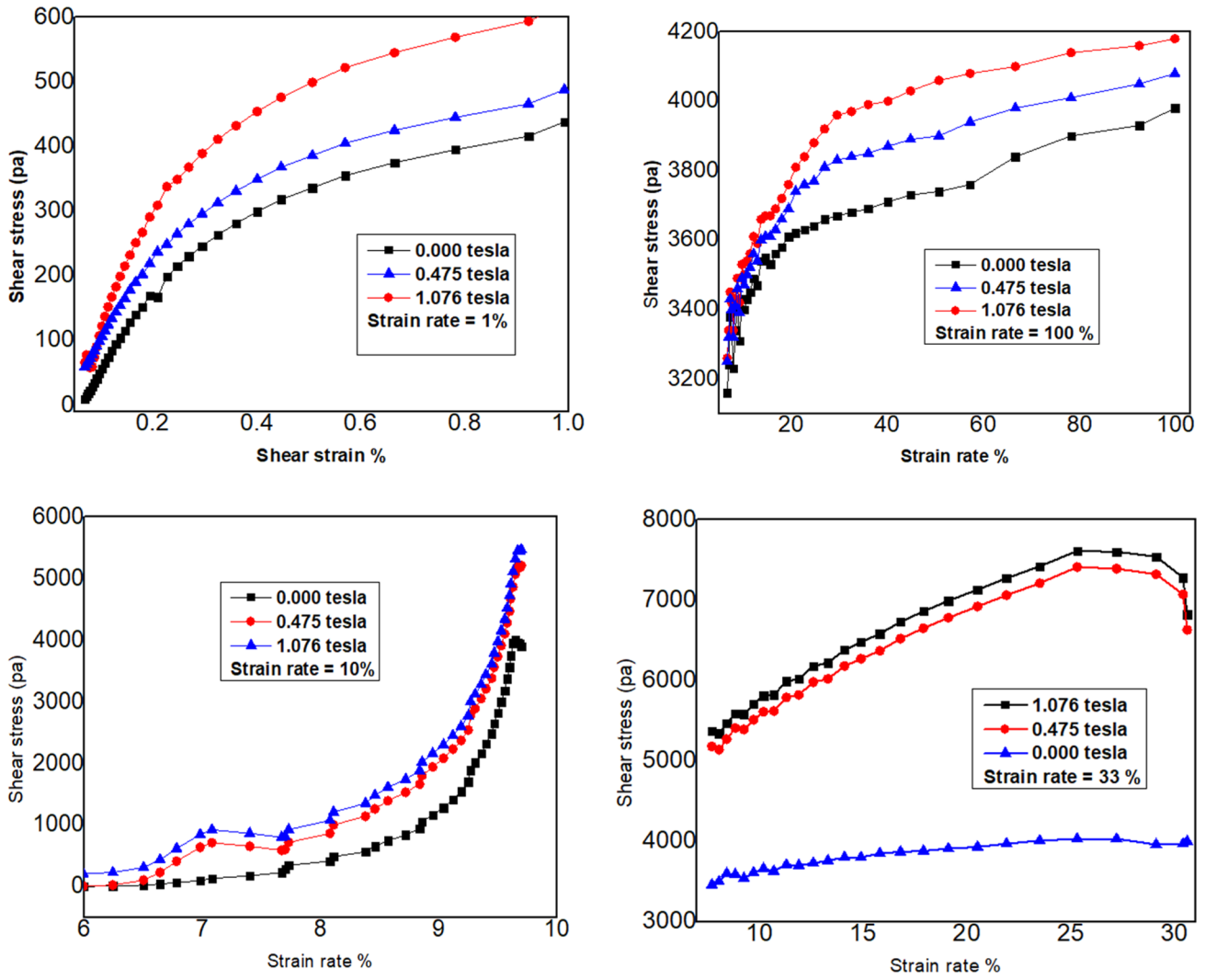

Fig. 13 Shear stress of $ZnFe_2O_4$ ferrofluid under the influence of different magnetic fields and at the strain amplitudes 1%, 10%, 33%, and 100%

henceforth, the particles are segregated from the aggregates. The destruction of the aggregate leads to formation of low magnetoviscosity. The shear stress is higher under the application of 1.076 T at 33% strain, and the shear force is decreased when the magnetic field is decreased to 0.475 T and when it is absent. Elastic limit is exceeded under the application of 33% strain; this occurred, because the shear stress reached a critical point; at this point, the field-induced structure completely breaks at high strain region; this diminished the resistance to fluid flow. At low strain rate region, the nanofluid revealed rapid increase in the shear stress, and this behavior could be well represented by Bingham law [56]

$$\tau = \tau_B + \eta_P \gamma, \tag{16}$$

where τ is shear stress, τ_B is yield stress, η_P is field-dependent viscosity, and $\dot{\gamma}$ is the shear rate.

In the absence of magnetic field (0.000 T), low shear stress is formed, but high shear stress is formed when magnetic field is applied. This result indicates the dependency of shear stress on the magnetization and applied magnetic field. Low yield stress is formed when strain rate 1% is applied; this accounts for the formation of high magnetoviscosity which is formed due to enhanced magnetization of the fluid particles. The magnetization of the interacting particles is decreased as the value of the strain rate is increased. This effect is attributed to increase in the deformation of the particle shape and/or increasing volume or length of the particle. If the strain is increased further, the particle is deformed at the critical point; this leads to the destruction of the chain

structure of the fluid particles. We see that the yield stress is increased in a quadratic mode as the applied magnetic field is increased, and the yield stress is represented as [4]

$$\tau_{y=} \propto \mu_o \mu_{c(\beta H)^2}, \tag{17}$$

where μ_0 is the permeability of the vacuum, μ_c is the relative permeability of the carrier fluid, and β is the contrast factor which is defined as [4]

$$\beta = \frac{\mu_p - \mu_c}{\mu_p + 2\mu_c}, \tag{18}$$

where μ_p is the relative permeability of the particle. The contrast factor β of Fe_3O_4-based magneto rheological fluid is around 2.7 [82]. The magnitude of the contrast factor β of other magneto rheological fluid varies from 2 to 3, depending on the respective nano-materials [82]. The respective yield stress is field independent in the presence higher magnetic fields strength within the magnetic saturation limit [4]

$$\tau_y \propto \mu_{oM_s^2}, \tag{19}$$

where M_s is the saturation magnetization and μ_0 is the permeability of the vacuum.

4 Conclusion

Soft spherical magnetic particles which form Fe-phase in trivalent state and exhibit FCC framework are synthesized. We examined the complex magneto-viscous and magneto-viscoelastic effect of the nano-sized zinc ferrite ferrofluid synthesized using co-precipitation technique. The rheological properties of the fluid were investigated at strain amplitude 1%, 10%, 33%, and 100% in the absence and presence of magnetic field. In the presence of magnetic field at strain 1% and 10%, low deformation is formed, and this leads to the formation of improved and better rheological systems. At strain 33%, the rheological system of the fluid is partially weakened; this occurred due to partial deformation of the field-induced structure. Large deformation is formed at strain 100%; this largely weakened the rheological function of the system. At low strain, high complex magnetoviscosity is formed; this is formed due to formation of enhanced magnetic aggregate which is not susceptible of destroying by low strain. At high strain, the complex magnetoviscosity is diminished; this occurred due to destruction of the magnetic aggregate; the aggregate is destroyed, because the large strain is highly susceptible of destroying the magnetic structure. At low strain rate, low shear stress is formed, the low stress is not susceptible of destroying field-induced structure, and this results in the formation of high magnetoviscosity, but at high strain rate, high shear stress is formed, the high stress is susceptible of destroying the field-induced structure, and this effect supports the formation of low magnetoviscosity. Low torque is formed under the application of strain rate 1%, and the low torque slowly rotates the magnetic field in a manner that cannot destroy the field-induced structure. However, at high strain, high torque is formed, and the high torque highly rotates the magnetic field in a manner that can destroy the field-induced structure. A steady-state flow is formed when low relaxation modulus is applied. At low strain amplitude, the storage modulus is greater than the storage modulus formed at high strain rate; this implies the formation of larger elastic structure at low strain application. The sample was characterized by Transmission Electron Microscopy (TEM) and X-ray diffraction which confirmed the formation of spherically shaped nanoparticle and single-phase cubic spinel. The particle is soft magnetic due to its low coercivity. Since this reported research is limited to purely experimental findings, we therefore propose in our future work the implementation of accurately established size-dependent elasticity mathematical models such as nonlocal strain gradient model and nonlocal strain-driven gradient model. The model will be used to analyze the physico-mechanical properties, such as elasticity, hardness, and softness of the conceived zinc ferrite structure.

Declarations

Conflict of interest The authors have no conflicts of interest.

References

1. P. Yang, M. Yu, H. Loo, J. Fu, H. Qu, Y. Xie, Improved rheological properties of dimorphic magnetorheological gels based on flower-like carbonyl iron particles. Appl. Surf. Sci. **416**, 772–466 (2017)
2. C.S. Maurya, C. Sarkar, Rheological and creep and recovery behavior of carbonyl iron water-based magnetorheological gel using laponite as an additive and oleic acid as surfactant. Rheol. Acta **61**, 99–110 (2022)
3. A.A. Ibiyemi, G.T. Yusuf, A. Olusola, Influence of temperature and magnetic field on rheological behavior of ultra-sonicated and oleic acid coated cobalt ferrite ferrofluid. Phys. Scr. **96**, 125842 (2021)
4. A. Chattopadhyay, S. Samanta, R. Srivastava, R. Mondal, P. Dhar, Elemental substitution tuned magneto-elastoviscous behavior of nanoscale ferrite MFe2O4 (M = Mn, Fe Co, Ni) based complex fluids. J. Magn. Magn. Mater. **149**, 265622 (2019)
5. M.H. Prasad, K.V. Gangadharan, Synthesis and magneto mechanical properties of MR grease. Int. J. Eng. Res. Technol. **3**(5), 2369–2372 (2014)
6. Y. Yang, L. Li, G. Chen, W. Li, Magnetorheological properties of aqueous ferrofluid. J. Soc. Rheol. **24**(1), 25–31 (2005)
7. T. Mitsumaka, T. Okazaki, Magnetization-induced reduction in dynamic modulus of polyurethane elastomers loaded with ferrite. Jpn. J. Appl. Phys. **46**(7A), 4220–4224 (2007)

8. E.G. Zukas, J.W. Taylor, Effect of strain aging on the dynamic elastic-plastic properties of iron materials at high strain rates. Inst. Phys. Conf. **21**, 177–185 (1974)
9. M. Heine, J. de Vicente, D.J. Klingenberg, Thermal transport in sheared electro- and magnetorheological fluids. Phys. Fluids **18**, 023301 (2006)
10. K.J. Solis, J.E. Martin, Isothermal magnetic advection: creating functional fluid flows for heat and mass transfer. Appl. Phys. Lett. **97**, 034101 (2010)
11. W. Kordonski, D. Golini, Multiple application of magnetorheological effect in high precision finishing. J. Intell. Mater. Syst. Struct. **13**, 401–404 (2002)
12. S. Jha, V.K. Jain, Design and development of the magnetorheological abrasive flow finishing (MRAFF) process. Int. J. Mach. Tools Manuf. **44**, 1019–1029 (2004)
13. W.I. Kordonski, A.B. Shorey, M. Tricard, Magnetorheological Jet (MR JetTM) finishing technology. J. Fluids Eng. **128**, 20–26 (2006)
14. J. Liu, G.A. Flores, R. Sheng, J. Magn. Magn. Mater. **225**, 209–217 (2001)
15. F. Donado, J.L. Carrillo, M.E. Mendoza, J. Phys. Condensed Matter. **14**, 2153–2157 (2002)
16. D.H. Read, J.E. Martin, Anal. Chem. **82**(5), 2150–2154 (2010)
17. D.H. Read, J.E. Martin, Adv. Funct. Mater. **20**(10), 1577–1584 (2010)
18. S.G. Sherman, A.C. Becnel, N.M. Wereley, J. Magn. Magn Mater. **380**, 98–104 (2015)
19. N. Rezlescu, C. Doroftei, E. Rezlescu, P.D. Popa, Sens. Actuators B Chem. **115**, 589–595 (2006)
20. V.K. Sankaranarayanana, O. Prakasha, R.P. Panta, M. Islam, Lithium ferrite nanoparticles for ferrofluid applications. J. Magn. Magn. Mater. **252**, 7–9 (2002)
21. A. Kumar, A. Annveer, M. Aroraa, M.S. Yadaf, R.P. Panta, Induced size effect on nickel doped nickel zinc ferrite nanoparticles. Phys. Procedia **9**, 20–23 (2010)
22. M. Shinkai, J. Biosci. Bioeng. **94**, 606–613 (2002)
23. D.H. Chen, Y.Y. Chen, Synthesis of barium ferrite ultrafine particles by co-precipitation in the presence of polyacrylic acid. J. Colloid Interface Sci. **235**, 9–14 (2001)
24. R. Monsef, M. Ghiyasiyan-Arani, M. Salavati-Niasari, Design of magnetically recyclable ternary Fe_2O_3/$EuVO_4$/g-C_3N_4 nanocomposites for photocatalytic and electrochemical hydrogen storage. ACS Appl. Energy Mater. **4**(1), 680–695 (2021)
25. S. Zinatloo-Ajabshir, M. Salavati-Niasari, Preparation of magnetically retrievable $CoFe_2O_4$@SiO_2@$Dy_2Ce_2O_7$ nanocomposites as novel photocatalyst for highly efficient degradation of organic contaminants. Compos. B Eng. **174**, 106930 (2019)
26. A. Goldman, *Modern Ferrite Technology*, 2nd edn. (Springer, New York, 2006)
27. J. Vicente, J.D.G. Durán, A.V. Delgado, Electrokinetic and viscoelastic properties of magnetorheological suspensions of cobalt ferrite. Colloids Surf. A Physicochem. Eng. Aspect. **19**(5), 181–188 (2001)
28. D.C. Silva, K.S. Neto, J.A.H. Coaquira, P.P. Araujo, D.O.S. Cintra, E.C.D. Lima, L.R. Guilherme, E. Mosiniewicz-Szablewsk, P.C. Morais, Magnetic characterization of vermiculite-based magnetic nanocomposites. J. Non-Crystall. Solids **356**, 2574–2577 (2010)
29. T. Hyeon, Y. Chung, J. Park, S.S. Lee, Y.-W. Kim, B.H. Park, Synthesis of highly crystalline and monodisperse cobalt ferrite nanocrystals. J. Phys. Chem. B **106**, 6831–6833 (2002)
30. Z.G. Zheng, X.C. Zhong, Y.H. Zhang, H.Y. Yu, D.C. Zeng, Synthesis, structure and magnetic properties of nanocrystalline $Zn_xMn_{1-x}Fe_2O_4$ prepared by ball milling. J. Alloys Compd. **466**(1–2), 377–382 (2008)
31. F.M.L. Oliveira, S.R. Avelino, M.T.A. Eloi, P.P. Gravina, K. Skeff-Neto, E.C.D. Lima, P.C. Morais, The influence of the nanoparticles dilution upon the structure of molecular-coated magnetic fluid. J. Non-Crystall. Solids **352**(32–35), 3689–3691 (2006)
32. X.-H. Li, Xu. Cai-Ling, X.-H. Han, L. Qiao, T. Wang, F.-S. Li, Synthesis and magnetic properties of nearly monodisperse $CoFe_2O_4$ nanoparticles through a simple hydrothermal condition. Nanoscale Res. Lett. **5**(6), 1039–1044 (2010)
33. J. Vicente, A.V. Delgado, R.C. Plaza, J.D.G. Duran, F. Gonzalez-Caballero, Stability of cobalt ferrite colloidal particles. Effect of pH and applied magnetic fields. Langmuir **16**, 7954–7961 (2000)
34. S. Odenbach, Microstructure and rheology of magnetic hybrid materials. Arch. Appl. Mech. **86**, 269–279 (2016)
35. N. Gautam, G. Thirupathi, R. Singh, Magnetoviscosity of paraffin-based barium ferrite ferrofluid. IEEE Trans. Magn. **52**, 4600204 (2016)
36. T. Prakash, G.V.M. Williams, J. Kennedy, S. Rubanov, Formation of magnetic nanoparticles by low energy dual implantation of Ni and Fe into SiO_2. J. Alloy. Compd. **667**, 255–261 (2016)
37. P.P. Murmu, J. Kennedy, B.J. Ruck, G.V.M. Williams, A. Markwitz, S. Rubanov, A.A. Suvorova, Effect of annealing on the structural, electrical and magnetic properties of Gd-implanted ZnO thin films. J. Mater. Sci. **47**, 1119–1126 (2012)
38. J. Kennedy, G.V.M. Williams, P.P. Murmu, B.J. Ruck, Intrinsic Magnetic order and inhomogeneous transport in Gd-implanted zinc oxide. Phys. Rev. B **88**, 214423 (2013)
39. T. Prakash, G.V.M. Williams, J. Kennedy, S. Rubanov, High spin-dependent tunneling magnetoresistance in magnetite powders made by arc-discharge. J. Appl. Phys. **120**, 123905 (2016)
40. S.A. Faghidian, Flexure mechanics of nonlocal modified gradient nano-beams. J. Comput. Design Eng. **8**(3), 949–959 (2021)
41. S.A. Faghidian, Contribution of nonlocal integral elasticity to modified strain gradient theory. Eur. Phys. J. Plus **136**, 559 (2021). https://doi.org/10.1140/epjp/s13360-021-01520-x
42. S.A. Faghidian, Two-phase local/nonlocal gradient mechanics of elastic torsion. Math. Methods Appl. Sci. (2020). https://doi.org/10.1002/mma.6877
43. S.A. Faghidian, Higher-order mixture nonlocal gradient theory of wave propagation. Math. Methods Appl. Sci. (2020). https://doi.org/10.1002/mma.6885
44. S.A. Faghidian, K.K.K. Żur, J.N. Reddy, A mixed variational framework for higher-order unified gradient elasticity. Int. J. Eng. Sci. **170**, 103603 (2022)
45. M. Hassanpour, H. Safardoust-Hojaghan, M. Salavati-Niasari, Degradation of methylene blue and Rhodamine B as water pollutants via green synthesized Co_3O_4/ZnO nanocomposite. J. Mol. Liq. **229**, 293–299 (2017)
46. M. Ghiyasiyan-Arania, M. Salavati-Niasaria, S. Naseh, Enhanced photodegradation of dye in waste water using iron vanadate nanocomposite; ultrasound-assisted preparation and characterization. Ultrason. Sonochem. **39**, 494–503 (2017)
47. S. Zinatloo-Ajabshir, S. Mortazavi-Derazkola, M. Salavati-Niasari, Nd2O3 SiO2 nanocomposites: a simple sonochemical preparation, characterization and photocatalytic activity. Ultrason. Sonochem. **42**, 171–182 (2018)
48. M. Panahi-Kalamuei, S. Alizadeh, M. Mousavi-Kamazani, M. Salavati-Niasari, Synthesis and characterization of CeO2 nanoparticles via hydrothermal route. J. Ind. Eng. Chem. **21**, 1301–1305 (2015)
49. F. Davar, M. Salavati-Niasari, Z. Fereshteh, Synthesis and characterization of SnO2 nanoparticles by thermal decomposition of new inorganic precursor. J. Alloys Compd. **496**(1–2), 638–643 (2010)
50. R. Monsef, M. Salavati-Niasari, Electrochemical sensor based on a chitosan-molybdenum vanadate nanocomposite for detection of

hydroxychloroquine in biological samples. J. Colloid Interface Sci. **613**(2022), 1–14 (2022)
51. M. Ajmal, A. Maqsood, AC conductivity, density related, and magnetic properties of $Ni_{1-x}Zn_xFe_2O_4$ ferrites with the variation of zinc concentration. Mater. Lett. **62**, 2077–2080 (2008)
52. J. Dhumal, S.S. Bandgar, M. Phadatare, G.S. Shahane, Superparamagnetic Fe-Mn ferrite nanoparticle for magnetic fluid hyperthermia. Int. J. Res. Anal. Rev. **6**(1), 1058–1066 (2019)
53. H. Anwar, A. Maqsood, I.H. Gul, Effect of synthesis on structural and magnetic properties of cobalt doped Mn-Zn nano ferrites. J. Alloys Compd. **626**, 410–414 (2015)
54. A.J. Rondinone, A.C.S. Samia, Z.J. Zhang, Characterizing the magnetic anisotropy constant of spinel cobalt ferrite nanoparticles. Appl. Phys. Lett. **76**, 3624 (2000)
55. V. Šepelák, I. Bergmann, A. Feldhoff, P. Heitjans, F. Krumeich, D. Menzel, F.J. Litterst, S.J. Campbell, K.D. Becker, Nanocrystalline nickel ferrite, $NiFe_2O_4$: mechanosynthesis, nonequilibrium cation distribution, canted spin arrangement, and magnetic behavior. J. Phys. Chem. C **111**(13), 5026–5033 (2007)
56. A. Mishra, S. Pathak, P. Kumar, A. Singh, K. Jain, R. Chaturvedi, D. Singh, G.A. Basheed, R.P. Pant, Measurement of static and dynamic magneto-viscoelasticity in facile varying pH synthesized $CoFe_2O_4$-based magnetic fluid. IEEE Trans. Magn. **55**(12), 4601107 (2019)
57. M. Chand, A. Shankar, A. Noorjahan, K. Jain, R.P. Pant, Improved properties of bidispersed magnetorheological fluids. R. Soc. Chem. Adv. **4**, 53960 (2014)
58. T. Gholami, M. Salavati-Niasari, S. Varshoy, Electrochemical hydrogen storage capacity and optical properties of $NiAl_2O_4$/NiO nanocomposite synthesized by green method. Int. J. Hydrogen Energy **42**(8), 5235–5245 (2017)
59. A.V. Dijken, E.A. Meulenkamp, D.V. Ilbergh, A. Meijerink, J. Lumin. **90**, 123 (2000). https://doi.org/10.1016/S0022-2313(99)00599-2
60. A. Manikandan, N.C.S. Selvam, L.J. Kennedy, R.T. Kumar, J.J. Vijaya, J. Nanosci. Nanotech. **13**, 2595–2603 (2013). https://doi.org/10.1166/jnn.2013.7357
61. S. Maensiri, C. Masingboon, B. Boonchom, S. Seraphin, A simple route to synthesize nickel ferrite (NiFe 2O4) nanoparticles using egg white. Scr. Mater. **56**, 797–800 (2007)
62. P. Priyadharsini, A. Pradeep, P. Sambasiva, G. Chandrasekaran, Structural, spectroscopic and magnetic study of nanocrystalline Ni-Zn ferrites. Mater. Chem. Phys. **116**, 207–213 (2009)
63. D. Padalia, U. Johri, M. Zaidi, Efect of cerium substitution on structural and magnetic properties of magnetite nanoparticles. Mater. Chem. Phys. **169**, 89–95 (2016)
64. P.P. Hankare, R.P. Patil, A.V. Jadhav, R.S. Pandav, K.M. Garadkar, R. Sasikala, A.K. Tripathi, Synthesis and characterization of nanocrystalline Ti- substituted Zn ferrite. J. Alloys Compd. **509**, 2160–2163 (2011)
65. I. Ahmad, S.A. Ansari, D.R. Kumar, Structural, morphological, magnetic properties and cation distribution of Ce and Sm co-substituted nano crystalline cobalt ferrite. Mater. Chem. Phys. **208**, 248–257 (2018)
66. A.A. Ibiyemi, G.T. Yusuf, O. Olubosede, A. Olusola, H.A. Akande, Photoelectric and magnetic properties of chemically synthesized Cd–Ni Ferrite nanomagnetic particles. Phys. Scr. **97**(2022), 025804 (2022)
67. E. Lemaire, A. Meuier, G. Bosis, J. Liu, D. Felt, P. Bashtovoi, N. Matoussevitch, J. Rheol. **39**, 1011 (1995)
68. K. Shah, J.-S. Oh, S.-B. Choi, R. Upadhyay, Plate-like iron particles based bidisperse magnetorheological fluid. J. Appl. Phys. **114**, 213904 (2013)
69. M.J. Pastoriza-Gallego, M. Pérez-Rodríguez, C. Gracia-Fernández, M.M. Piñeiro, Study of viscoelastic properties of magnetic nanofluids: an insight into their internal structure. Soft Matter **9**, 11690–11698 (2013)
70. L.J. Felicia, J. Philip, Magnetorheological properties of a magnetic nanofluid with dispersed carbon nanotubes. Phys. Rev. E **89**, 022310 (2014)
71. C. Huang, J. Yao, T. Zhang, Y. Chen, H. Jiang, D. Li, Damping application of ferrofluid: a review. J. Magn. **22**(1), 109–121 (2017)
72. S. Samouhos, G. McKinley, Carbon nanotube–magnetite composites, with applications to developing unique magnetorheological fluids. J. Fluids Eng. **129**, 429–437 (2007)
73. R.E. Rosenzweig, *Ferro-hydrodynamics* (Cambridge University Press, Cambridge, 1985)
74. G. Noorjahan, A. Basheed, K. Jain, S. Pathak, R.P. Pant, Dipolar interaction and magneto viscoelasticity in nanomagnetic fluid. J. Nanosci. Nanotechnol. **17**, 1–6 (2017)
75. B.V.S. Iyer, V.V. Yashin, A.C. Balazs, Dynamic behavior of dual cross-linked nanoparticle networks under oscillatory shear. N. J. Phys. **16**, 075009 (2014)
76. L.A. Powell, W. Hu, N.M. Wereley, Magnetorheological fluid composites synthesized for helicopter landing gear applications. J. Intell. Mater. Syst. Struct. **24**, 1043–1048 (2013)
77. G. Paul, P.K. Das, I. Manna, Synthesis, characterization and studies on magneto-viscous properties of magnetite dispersed water based nanofluids. J. Magn. Magn. Mater. **404**, 29–39 (2016)
78. M. Hassan, A. Zeeshan, A. Majeed, R. Ellahi, Particle shape effects on ferrofuids flow and heat transfer under influence of low oscillating magnetic field. J. Magn. Magn. Mater. **443**, 36–44 (2017)
79. J.A. Ruiz-López, Z.W. Wang, R. Hidalgo-Alvarez, J. de Vicente, Simulations of model magnetorheological fluids in squeeze flow mode. J. Rheol. **61**, 871–881 (2017)
80. Y. Tong, X. Dong, M. Qi, High performance magnetorheological fluids with flower-like cobalt particles. Mater. Struct. **26**, 025023 (2017)
81. A.Y. Zubarev, J. Fleischer, S. Odenbach, Statistical mechanics and its applications. Phys. A **358**, 475 (2005)
82. D.Y. Borin, A.Y. Zubarev, D.N. Chirikov, S. Odenbach, J. Phys. Condensed Matter **26**, 406002 (2014)
83. J. Mohapatra, A. Mitra, D. Bahadur, M. Aslam, Surface controlled synthesis of MFe2O4 (M= Mn, Fe Co, Ni and Zn) nanoparticles and their magnetic characteristics. Cryst. Eng. Commun. **15**(3), 524–532 (2013)